ACS Catalysis
Research Article
Cite This: *ACS Catal.* 2019, 9, 269−285
pubs.acs.org/acscatalysis

Operando Structure Determination of Cu and Zn on Supported MgO/SiO_2 Catalysts during Ethanol Conversion to 1,3-Butadiene

William E. Taifan,[†,∇,○] Yuanyuan Li,[‡,∇] John P. Baltrus,[§] Lihua Zhang,[∥] Anatoly I. Frenkel,[‡,⊥] and Jonas Baltrusaitis[*,†]

[†]Department of Chemical and Biomolecular Engineering, Lehigh University, B336 Iacocca Hall, 111 Research Drive, Bethlehem, Pennsylvania 18015, United States

[‡]Department of Materials Science and Chemical Engineering, Stony Brook University, Stony Brook, New York 11794, United States

[§]National Energy Technology Laboratory, U.S. Department of Energy, 626 Cochrans Mill Road, Pittsburgh, Pennsylvania 15236, United States

[∥]Brookhaven National Laboratory, Center for Functional Nanomaterials, Upton, New York 11973, United States

[⊥]Division of Chemistry, Brookhaven National Laboratory, Upton, New York 11973, United States

Supporting Information

ABSTRACT: The electronic structure and reactivity of Cu- and Zn-promoted wet-kneaded MgO/SiO_2 catalysts was interrogated during ethanol reaction to 1,3-BD. A multimodal nature of characterization, including *in situ* or *operando* X-ray, electron, light spectroscopies, and steady state reactivity measurements demonstrated critical information on the temporal evolution of the catalyst active sites including key measurements performed in *operando* conditions using synchrotron techniques (EXAFS and XANES). *In situ* DRIFT spectroscopy allowed decoupling of the aldol condensation and dehydrogenation reactive steps due to the promotion with enhanced ability to carry out aldol condensation, as correlated with the steady state reactivity experiments. *In situ* UV−vis spectroscopy presented a complex picture of the adsorbates with $\pi-\pi^*$ electronic transitions due to the allylic cations, cyclic or aromatic species while also suggesting oligomeric CuO species were formed. *Operando* X-ray measurements combined with *ab initio* multiple scattering modeling performed as a function of temperature identified a transient intermediate assigned to a 4-fold coordinate Cu species that was key leading to increase in Cu−Cu pair number. We identified two types of Zn pairs, namely Zn−O and Zn−Mg, during X-ray analysis under operating conditions. With Zn nearly 6-coordinated when in the vicinity of Mg while Zn−O species coordinated to nearly 4 nearest neighbors. The data suggest that such supported catalyst deactivation might proceed not only via carbon coking mechanism but also through the dispersed Cu site diffusion and growth due to the nearest neighbor oxygen atoms loss. The results presented suggest intermediates for segregation/deactivation mechanisms for a broader set of supported Cu and Zn catalysts used for alcohol upgrading catalytic reactions.

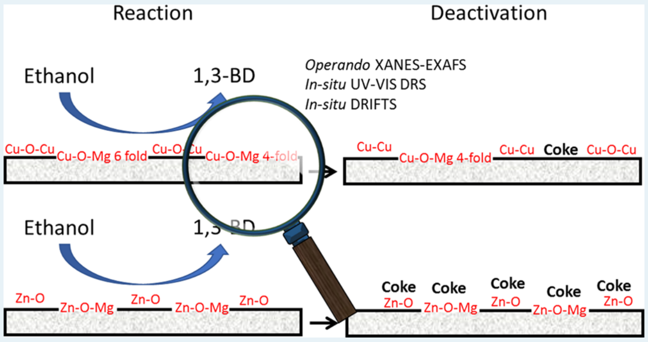

KEYWORDS: *ethanol, 1,3-butadiene, MgO/SiO_2, operando, spectroscopy, XANES, EXAFS*

1. INTRODUCTION

Catalytic conversion of ethanol to 1,3-butadiene (ETB) is a promising green and renewable route for obtaining a commodity chemical that does not utilize a conventional petroleum-based feedstock.[1] The feedstock and technological process landscape in 1,3-butadiene (1,3-BD) production is undergoing changes due to the distinct industry shift from oil to C_4 hydrocarbon lean shale gas.[2] In this regard, ethanol is a very interesting *platform* molecule due to its steadily increasing production from biomass.[1] Two classes of catalysts have been used for ethanol conversion to 1,3-BD, namely ZrO_2-based and MgO/SiO_2-based (Lebedev catalyst).[3] The former have thoroughly been investigated using a combination of computational and spectroscopic methods[4,5] while the latter lack suitable spectroscopic characterization.[3] The overall reaction mechanism on MgO/SiO_2 is currently debated,[3,6−8] and several recent attempts have been made to elucidate it.[6,9−12] These studies pointed toward aldol condensation as the most energetically favorable C−C bond formation mechanism, except for Chieregato et al., who suggested that a C−C bond was formed via interaction of ethanol/acetaldehyde through a stable carbanion intermediate.[9] The rate-determin-

Received: September 2, 2018
Revised: November 21, 2018
Published: November 28, 2018

DOI: 10.1021/acscatal.8b03515
ACS Catal. 2019, 9, 269−285

ing step was found to be ethanol dehydrogenation[6,11] since an efficient dehydrogenating site was not present in MgO/SiO_2 catalysts. This suggests that an effective catalyst must possess multifunctional, i.e. acidic, basic, and redox, sites. MgO/SiO_2 catalysts are promoted with transition metal (oxides) to improve their dehydrogenation capability[2,13−17] where the choice of transition metal used as a promoter is determined by its dehydrogenation capability.[18−20] Au,[21,22] Ag,[23,24] and Cu[25,26] have been utilized to enhance the 1,3-BD yield.[2,27,28] Zn is another promoter that has been utilized to improve the yield of 1,3-BD.[13,15,29−31] The promotional effect was reported to originate from the improved availability of both Lewis acid sites and redox sites.[3,15] While Au and Ag promoters present economic constraints due to their high costs, Cu and Zn are relatively inexpensive and present an alternative for an efficient catalyst design. The work reported here provides new insights on the structure and reactivity of these sites under operating conditions.

Several theoretical and ultrahigh vacuum (UHV) studies have been conducted on Cu-based catalysts to determine the structure of the active sites[32−39] but very few under operating conditions. UHV characterization and DFT revealed formation of isolated or clustered Cu^0 phases on the MgO surface[32,33] or a solid solution that contains Cu−Mg and Cu−O−Mg pairs.[34] The formation of reduced Cu clusters on the surface was confirmed by Colonna et al. where Cu clusters, as evident by Cu−Cu distance (2.55 Å), were observed as a thin layer on MgO using X-ray Absorption Near Edge Structure (XANES) during the UHV evaporation−deposition synthesis.[35] In a separate study, in addition to the observed Cu atoms on the MgO surface, both UHV XANES and DFT identified the formation of a solid solution between Cu and MgO.[36,37] Larger charge transfer resulting in a strong ionic bond was observed when Cu was coordinated next to a defective MgO surface.[38,39] This shorter bond was due to the electron stabilization provided by the Cu atom.[38,39] UHV XANES of several transition metal-promoted MgO catalysts utilized for CH_3OH and RCH_2Z (where R = H and CH_3; Z = CN, COR′, and COOR″) coupling reactions confirmed the formation of Cu-MgO solid solution at 80 K and suggested that an octahedral coordination of the Cu species due to the pre-edge peak associated with 1s → 3d transition was very small. This observation was accompanied by the extended X-ray absorption fine structure (EXAFS) analysis of the Cu−O and Cu−Mg atomic distances, 2.01 and 2.98 Å, respectively, suggesting the formation of solid solution between Cu and MgO. Thus, a variety of active copper sites can be present under operating conditions,[28,40−42] but very few studies, notably Angelici et al.,[26,28] attempted to decouple their reactivity during 1,3-BD formation or investigate the temperature effect on Cu site composition under reactive conditions.[28] ZnO/SiO_2 has been used as a model catalyst for many reactions, such as water−gas shift and methanol formation reaction,[43] but X-ray based catalytic site characterization during ethanol-to-1,3-BD are not existent to the best of our knowledge.[13,15,16] *In situ* XAS and UV−vis of this catalyst further showed the relevance of the precursor drying steps during the synthesis and that Zn was present both as a silicate (hemimorpite) and ZnO bulk phase at 10% Zn loading.[43] Ambient UV−vis and TEM studies of a 1% ZnO/MgO catalyst demonstrated the formation of a highly dispersed ZnO layer which had high activity for CO oxidation, affected by the quantum-confinement effect.[44]

In this work, we performed a comprehensive characterization on both Cu- and Zn-promoted MgO/SiO_2 catalysts. The promotion effect on the catalyst structure was studied by bulk and *in situ* surface characterization techniques such as TEM, XRD, *in situ* DRIFTS and UV−vis (section 3.1). Section 3.2 discusses in detail the changes in the steady state reactivity of the catalyst when transition metals are used as promoters. Mechanistic reactivity changes due to the catalyst promotion with transition metal oxides are detailed by DRIFTS experiments in section 3.3.1, while the changes in the Cu and Zn local structure are summarized in the *in situ* UV−vis and *operando* XANES sections 3.3.2 and 3.3.3, respectively. Conclusions that are complementary, if not contradictory, to those available in the literature[28] were reached for Cu-promoted MgO/SiO_2 while new insights on the coordination of Cu and Zn were obtained for Zn-promoted MgO/SiO_2 catalysts from X-ray absorption spectroscopy data under operating conditions.

2. EXPERIMENTAL METHODS

2.1. Catalyst Synthesis.

The wet-kneaded (WT) MgO/SiO_2-support catalyst was prepared using the method used in the previous work.[11] Briefly, magnesium hydroxide, $Mg(OH)_2$, thermally precipitated from magnesium nitrate hexahydrate (Sigma), was wet-kneaded with fumed SiO_2 (Cabot). The corresponding amounts of SiO_2 and $Mg(OH)_2$ were wet-kneaded in deionized water for 4 h, centrifuged, and dried overnight at room temperature. The oxide mass ratio was chosen to be 1:1 ($MgO:SiO_2$) since this was previously described as an optimum ratio.[2,14,45] For the unpromoted catalyst, the support was further dried at 80 °C overnight, while this step was not included for the promoted catalyst synthesis. Following drying at ambient conditions, the catalyst was impregnated with transition metal promoters, i.e. copper and zinc salts. Copper nitrate trihydrate (Alfa Aesar) and zinc nitrate hexahydrate (Sigma) were used. The Cu concentration was selected to be 1%, based on work by Angelici et al.[14,28] while the Zn loading was 4% based on the work by Larina et al.[15] The thermal treatment that followed was done according to the method previously described.[14,15,28] As a reference, 3% CuO/MgO (CuMg), 3% ZnO/MgO (ZnMg), 3% CuO/SiO_2 (CuSi), and 3% ZnO/SiO_2 (ZnSi) catalysts were synthesized using an incipient-wetness impregnation method; the synthesized $Mg(OH)_2$ was used for the MgO support, while fumed silica (Cabot) was used for the SiO_2 support.

2.2. Steady State Reactivity Studies.

The steady state catalytic tests were done in a Microactivity-Reference fixed-bed reactor from PID Eng Tech (Spain). A quartz tube was used as a reactor with quartz wool to support the catalyst bed (0.1 g; sieved to 100−150 μm particle size to prevent excessive pressure drop while eliminating any transport effects). Additional SiO_2 powder (Sigma) was used to increase the bed length to maintain the plug flow conditions. SiO_2 powder alone showed no conversion. Ethanol was delivered into the reactor by bubbling He gas through a chilled ethanol saturator at 55 mL/min total flow. The reactor hotbox temperature was set at 100 °C to prevent any vapor condensation. The bubbler temperature was varied to manipulate the overall weight hourly space velocity (WHSV). Prior to the reaction, the catalyst was activated by heating it up to 500 °C at a rate of 10 K/min in He and then held at that temperature for 1 h under 30 mL/min He flow. The reaction was run at 350−450 °C where reactant was fed downstream into the reactor. *In situ* surface site poisoning study was performed by concurrently flowing ethanol and either CO_2, propionic acid, or NH_3. After ethanol reaction was equilibrated the probe molecule was flown simultaneously to detect the change in the principal (by)-product formation rates. The vapor phase products were analyzed using GC-FID equipped with a Restek RT-Q-Bond column. The principal ethanol reactant products, i.e. ethylene, acetaldehyde, and 1,3-BD, were quantified based on the calibration carried out using a standard reference mixture (Praxair).

2.3. Catalyst Characterization. Transition metal promoter concentrations, in weight %, of Cu- and Zn-promoted MgO/SiO_2 catalysts were determined using Inductively Coupled Plasma-Optical Emission Spectroscopy (ICP-OES, PerkinElmer Optima 2000 DV). About 10 mg of catalyst was digested in 40 mL of solution containing 1:1:1 H_2O, HCl, and HNO_3. Bulk Cu concentration was found to be 0.8%, similar to that used by Angelici et al.[14,28] while that of Zn was 2.5%, close to that reported by Larina et al.[15]

The XPS measurements were carried out with a PHI 5600ci instrument using a nonmonochromatized Al Kα X-ray source. The pass energy of the analyzer was 58.7 eV, the acquisition area had a diameter of ~800 μm, and the scan step size was 0.125 eV. Binding energies were corrected for charging by referencing to the C 1s peak at 284.8 eV. Atomic concentrations were calculated from the areas under individual high-resolution XPS spectra using manufacturer-provided sensitivity factors.

Bulk structural information on the catalysts was characterized using XRD. XRD patterns were obtained on a PANalytical Empyrean powder X-ray diffractometer using Cu $K_{\alpha1,2}$ with λ = 1.5418 Å operating at 45 kV. Measurements were carried out between $2\theta = 10°$ and 100° using a step size of 0.05°. The BET specific surface areas of the catalysts were determined by nitrogen adsorption at 77 K on a Micromeritics ASAP 2010 instrument. All samples were degassed under nitrogen flow at 623 K for 12 h before the measurements.

The morphology of the catalyst particles was investigated using a dedicated Scanning Transmission Electron Microscope (STEM) (Hitachi 2700C) operating at 200 kV.

2.4. *In Situ* and *Operando* Spectroscopy. *In situ* temperature-programmed diffuse reflectance infrared Fourier transform spectroscopy (DRIFTS) was performed using a Thermo Nicolet iS50 infrared spectrometer equipped with a Mercury−Cadmium−Tellurium (MCT) liquid nitrogen cooled detector, a Harrick Praying Mantis diffuse reflection accessory, and a ZnSe window. *In situ* UV−vis DRS experiments were performed using an Agilent Technologies Cary 5000 UV−vis−NIR to investigate the reactive ethanol conversion intermediate species and the transition metal promoter electronic structure. Briefly, about 30 mg of catalyst was pressed and loaded into the reaction cell, and the catalyst was activated using a protocol similar to that used in the steady state reactivity testing experiment. After the catalyst activation, spectra were taken at different temperatures to probe the dehydrated state of the catalysts. For *in situ* ethanol experiments, this was followed up by preadsorbing ethanol on the sample surface as a saturated vapor (saturator temperature at 4 °C) using 30 mL/min He as a carrier gas at catalyst temperature of 100 °C for 20 min. The catalyst was subsequently flushed with pure He at 30 mL/min for 40 min. Spectra were then continuously recorded every minute while the temperature was ramped up to 450 °C at 10 °C/min under ethanol flow with similar partial pressure. Unless stated otherwise, all spectra were referenced to the spectra obtained without the presence of ethanol at the corresponding temperatures. Analysis of the UV−vis spectra was done by deriving Tauc plots from the spectra. The Kubelka−Munk function was calculated from the absorbance of the UV−vis DRS. The edge energy (E_g) for allowed transitions was determined by finding the intercept between the straight line and the abscissa on the Tauc plot derived from the UV−vis spectra. In a similar manner, TP-DRIFTS experiments with probe molecules, i.e. CO_2 and NH_3, were performed. After activation at 500 °C, the catalyst temperature was decreased to 100 °C and CO_2 (Praxair) and 1% NH_3/N_2 were preadsorbed on the surface for 15 min, followed by inert for 45 min. The temperature was then ramped up to 450 °C with spectra being taken continuously.

Operando X-ray absorption spectroscopy (XAS) experiments were performed at the beamline BL2-2 at the Stanford Synchrotron Radiation Lightsource (SSRL), SLAC National Accelerator Laboratory. The Cu and Zn K-edge data were collected in transmission mode. For the measurements, the sample powder was loaded into a quartz tube with 0.9 mm inner diameter and 1.0 mm outer diameter, which was then mounted into the Clausen plug-flow reaction cell.[46] Ethanol vapor was delivered into the system using a temperature-controlled saturator to manipulate the space velocity. He was bubbled through the saturator and fed into the reactor. Prior to the spectroscopic study under reaction conditions, the catalyst was pretreated at 450 °C for 1 h under constant He flow. The *operando* measurements were performed at 100, 200, 300, and 400 °C under constant ethanol flow. After reactor temperature reached 400 °C, the system was allowed to equilibrate for 2 h and XAS spectra were repeatedly taken. The *operando* conditions were monitored by sampling the vapor-phase with a dedicated RGA mass spectrometer (RGA, Stanford research system). Standard reference compounds, CuO (Alfa Aesar), ZnO (Alfa Aesar), and Cu_2O (Alfa Aesar), and synthesized reference materials, i.e. CuMg, ZnMg, CuSi, and ZnSi, were pressed into the pellets and measured under ambient conditions.

3. RESULTS AND DISCUSSION

3.1. Catalyst Characterization. The transition metal content in each catalyst was determined using both ICP-OES and XPS to infer bulk and surface concentration, respectively. An agreement was found between the two characterization methods with ICP-OES determined Cu and Zn content of 0.8% and 2.5% virtually agreeing with those determined by XPS of 0.9% and 2.7% for each catalyst. These Zn and Cu concentrations are close to the intended high selectivity loading.[14,15] The starting support material, i.e. wet-kneaded MgO/SiO_2, possessed surface area of 120 m^2/g, while promoting the MgO/SiO_2 with transition metals led to an increase in the surface area. Zn and Cu-promoted samples exhibited surface area of 135 and 191 m^2/g, respectively. This increase in surface area was likely due to the impregnation step which was done before the support was calcined. The effect of calcination−impregnation order has previously been observed by Da Ros et al. with ZrZn-promoted MgO/SiO_2 catalysts.[16] This suggests that the metal promoters deposited via impregnation might also act as textural promoters, in addition to being electronic promoters.

The X-ray diffraction (XRD) patterns of the two promoted catalysts—CuMgSi and ZnMgSi—acquired under ambient conditions are shown in Figure 1 together with the unpromoted MgSi. The unpromoted sample exhibited prominent peaks at 37.4, 43.5, 63, 75, and 79° which were due to the periclase MgO. Amorphous silica was also present in the XRD pattern as evidenced by the broad band in the lower 2θ region of 20−30°. The wet-kneading of MgO and SiO_2 did not produce new bulk crystalline phases, in agreement with Angelici et al.[47] Shifts to lower value were observed for the 43.5° peak, suggesting the formation of solid solution, i.e. promoters incorporated into the lattice. Careful examination of the XRD pattern also showed that both Zn and Cu enhanced the intensity of the MgO peaks, suggesting changes in its crystalline structure. The enhanced crystallinity is very interesting, since the transition metal promoters must play a role in this structural change *(vide infra)*. As will be shown by STEM and XAS, addition of the promoters resulted in Cu−Mg, Zn−Mg solid solution, and very small nanoparticles that were not detected using XRD. We hypothesize that solid solution and nanoparticles impeded the interaction between MgO and SiO_2 and partially segregated the catalyst into a more crystalline MgO phase. For reference, several concentrations of ZnSi and ZnMg were prepared and analyzed with XRD (Figure S1). Neither ZnSi nor ZnMg showed any new crystalline phases being formed up to 5% loading. Similarly, no new peaks appeared in the CuMg while CuO clustering was observed on 5% CuSi (Figure S2), e.g. above the loading used for the working catalyst.

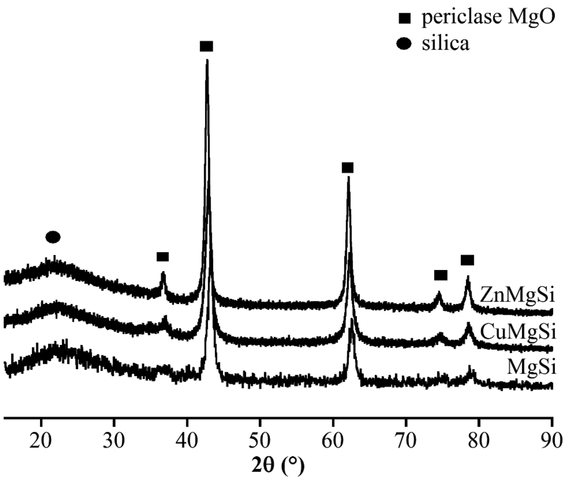

Figure 1. Comparison of XRD patterns between CuMgSi, ZnMgSi, and MgSi.

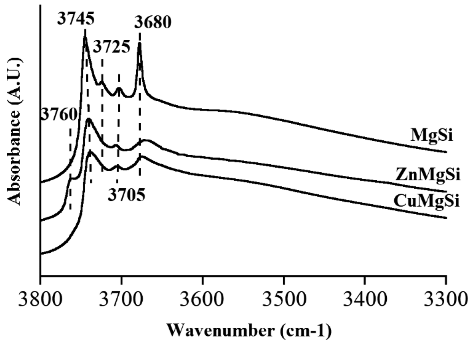

Figure 2. *In situ* dehydrated DRIFTS of OH region of MgSi, CuMgSi, and ZnMgSi. Spectra were taken at 100 °C under He flow after pretreatment at 500 °C for 1 h. Spectra are offset for clarity.

Figure 2 shows DRIFT spectra for dehydrated metal-promoted catalysts in the OH region, while that for the binary catalyst component compounds (ZnSi, ZnMg, CuSi, CuMg) is shown in Figure S3. The promoted MgSi catalysts show similar spectral features to the unpromoted MgSi. Detailed assignments of the four native OH groups can be found in the previous work.[11] Briefly, there are four prominent peaks on an MgO/SiO_2 catalyst, i.e. 3745 cm^{-1} assigned to both isolated MgO and silanol groups, 3725 and 3705 cm^{-1} ascribed to Mg−OH−Si with different OH coordination numbers and a 3680 cm^{-1} peak assigned to a magnesium silicate species. Promoting the MgSi with Cu or Zn significantly reduced and broadened the native silica and the WK-signature peaks, i.e. isolated silanol at 3745 cm^{-1} and Mg−O(H)−Si group at 3680 cm^{-1}. This suggests that both transition metal promoters, Cu and Zn, interact strongly with this OH group. Displacement with Zn further results in a new OH site, as shown by the emergence of a peak at 3760 cm^{-1}, which was previously assigned to the isolated hydroxyl group of MgO.[11,48] This highly isolated hydroxyl group might form from broken Mg−O−Si linkages due to the introduction of Zn suggesting Zn interaction with O−Mg.

The coordination and oxidation states of the metal promoters were further characterized using *in situ* UV−vis DRS under dehydrated conditions. Figure 3a shows a comparison between the Cu-promoted (CuMgSi) catalyst, MgSi, and reference binary materials, CuMg, CuSi, and bulk CuO. UV−vis DRS spectra of the bulk CuO are characterized by the presence of a charge transfer (CT) peak at ~251 nm and a peak at 570 nm. The CT peak is assigned to the ligand-to-metal CT (LMCT) from O^{2-} to Cu^{2+} in octahedral coordination.[40] The peak at 570 nm can be assigned to either surface plasmon resonance from Cu^0 or contributions from the d−d transition.[49] Furthermore, a peak at 235 nm is present on all supported Cu samples, while the peak at 270 nm is present only on a Mg-containing support. The former represents LMCT peaks for a very isolated Cu−O species,[28,40] while the latter has been assigned to an oligomeric Cu−O species.[40] The peak at 305 nm for CuSi is assigned to the oligomeric Cu−O species.[28] This reference sample (CuSi, Figure 3a) also exhibits a d−d transition peak at ~760 nm, indicative of Cu^{2+} species in a (distorted) octahedral field.[28] On the other hand, the CuMg reference exhibited an extra peak at 215 nm, possibly due to charge transfer from Mg^{2+} to the silica surface.[27] The CuMgSi catalyst exhibits a small peak at ~570 nm, which, as in the CuO reference case, is due to the presence of Cu^0. Dehydration under inert atmosphere is more likely to induce partial reduction on the catalyst.[28] In agreement, a known absorption peak in the 560−570 nm region is due to the plasmon resonance of metallic Cu nanoparticles.[49]

Tauc plots of the CuO standard and the catalyst (CuMgSi) were derived from the UV−vis DRS spectra and are shown in Figure S4. Using the method previously described by Bravo-Suarez et al.,[40] identification of the oligomer was made possible by correlating the number of species to the edge energy. The plot for CuMgSi was deconvoluted and isolated (0 nearest neighbors), and the oligomer species with edge energies of 3.86 and 3.51 eV, respectively, were identified. The Tauc plot indicates that the reference oxide CuO exhibits an edge energy of 1.26 eV, close to the previously determined values at 1.17 ±

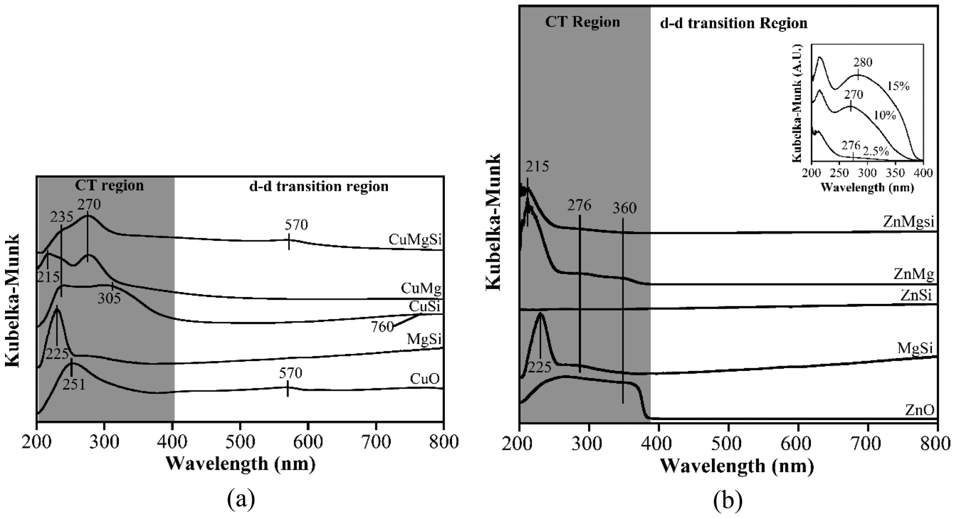

Figure 3. *In situ* UV−vis DRS spectra of (a) dehydrated CuMgSi catalyst referenced with Cu/MgO (CuMg), Cu/SiO_2 (CuSi), CuO, and MgSi; (b) dehydrated ZnMgSi catalyst referenced with Zn/MgO (ZnMg), Zn/SiO_2 (ZnSi), ZnO, and MgSi. Inset: UV−vis spectra of different loadings of Zn on MgO/SiO_2 catalysts.

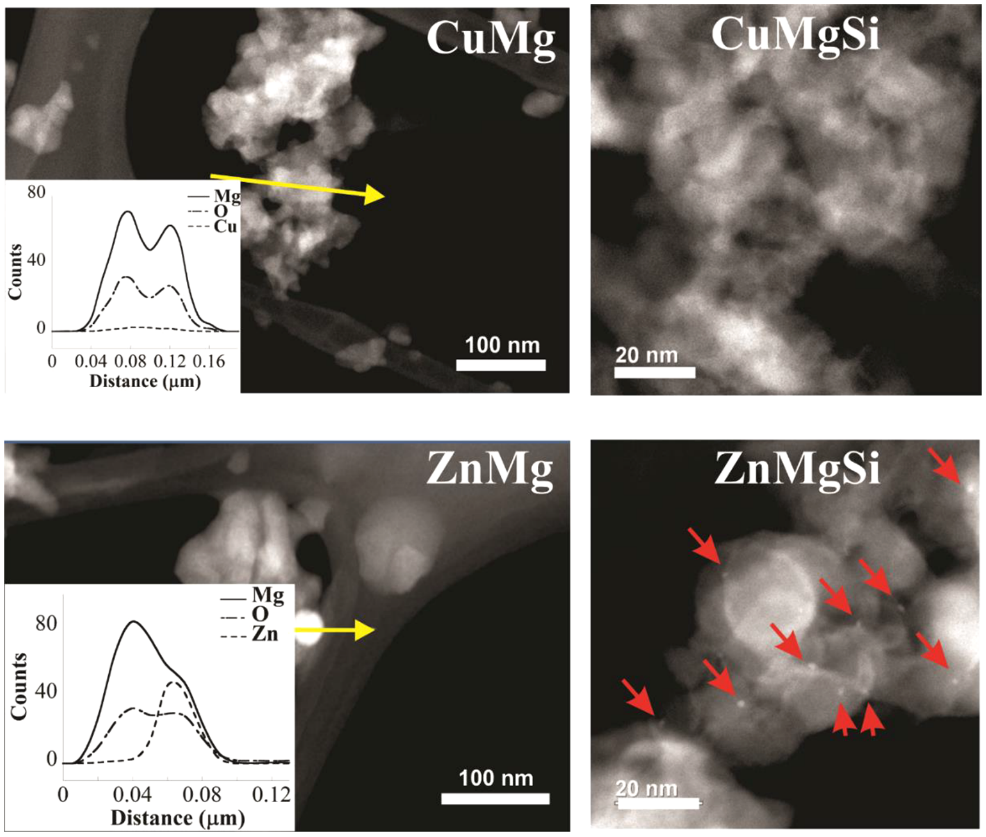

Figure 4. Scanning transmission electron microscopy images of ZnMg, ZnMgSi, CuMg, and CuMgSi samples. Energy dispersive spectroscopy profiles (smoothed) are also provided. Small ZnO nanoparticles are shown in ZnMgSi with red arrows.

0.06 eV.[40,50] The value for the isolated species in this work was higher than that reported for CuMgAl mixed oxide, reported to be ∼3 eV.[40] This is due to the coordination of the isolated CuO species to the surface. Using isolated CuO species and standard CuO (6 nearest neighbors), the coordination number, i.e. number of Cu−O−Cu bond, was determined to be 0.8.

The Zn-promoted catalyst UV−vis DRS spectra are shown in comparison with the reference samples, i.e., bulk ZnO, MgSi, ZnSi, and ZnMg, in Figure 3b. The ZnMgSi catalyst shows a small peak at 276 nm. This small peak is down shifted ∼100 nm, when compared to bulk ZnO at 360 nm. Additionally, ZnMgSi contains a peak at 215 nm, which resembles that of the CuMg UV−vis DRS spectrum. This CT peak appears in almost all Mg containing samples, except for CuMgSi. That peak was located at almost the same wavelength, ∼ 215 nm, for CuMg, ZnMg, and ZnMgSi, but shifted when MgSi support was measured, i.e. at 225 nm. This

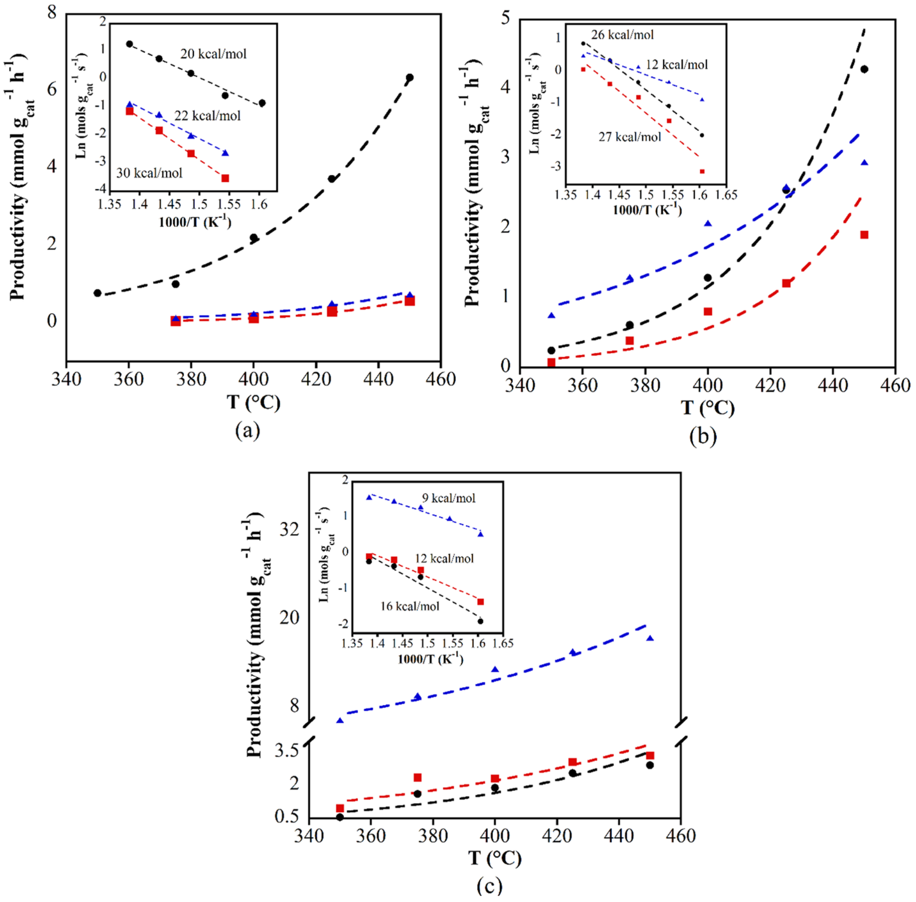

Figure 5. Productivity comparison of 1,3-BD (red ■), ethylene (black ●), and acetaldehyde (blue ▲) over (a) MgSi, (b) CuMgSi, and (c) ZnMgSi. Dotted lines are meant to guide the eyes. Insets: Arrhenius plots to show apparent activation energies of the three (by)products. Reactions were carried out between 325−450 °C, m_{cat} = 0.1 g, $p_{ethanol}$ = 1.8 kPa, total flow = 55 mL/min.

peak can be assigned to a charge transfer from Mg^{2+} to O^{2-}, where a shift is expected when MgO is wet-kneaded with SiO_2.[51] However, introducing Zn to the MgSi support seems to negate this shift and it reverts back to ∼215 nm. This phenomenon is consistent with DRIFTS data, as shown in Figure 2, where the OH peak at 3760 cm^{-1} disappeared when MgO was wet-kneaded to SiO_2 but reappeared when Zn is introduced to the surface. Figure 3b inset shows different Zn loadings on the wet-kneaded MgSi. At a higher loading, the peak at lower wavenumber, i.e. 215 nm, persists, while the ZnO peak started appearing at 270 and 280 nm for 10% and 15% Zn loadings, respectively. The shift in the CT peak is also followed by the shift in the edge energy. This shift with a higher Zn loading was also observed by Yoshida et al. on an SiO_2 support, although they describe this Zn site to have an electronic structure distinct from bulk ZnO, with XANES confirming that the ZnO is in a tetrahedral configuration.[52]

The reference ZnMg and ZnSi samples further aided in peak assignments of the UV−vis spectra of the ZnMgSi catalyst. In addition to the discussed 215 nm peak, the former exhibits two other peaks at 276 and 360 nm. The first peak could be associated with the defect Mg site of the catalyst, assigned to tricoordinated O^{2-} ions on corner sites, which is also encountered in the MgSi sample.[27,51,53] Along with the peak at lower wavelengths, 215−225 nm, these peaks are indicative of bulk MgO, also observed by Sels and co-workers.[27] The second peak is likely to be assigned to bulk ZnO based on the bulk ZnO reference spectra. The ZnMgSi catalyst, on the other hand, hardly shows any other peaks related to Zn-containing species. Chouillet et al. reported a similar observation, where UV−vis shows bands of a bulk ZnO phase in the limit of 1.4−4.4 nm particle size, confirmed by TEM.[43] To explore the possibility of the formed ZnO phase in the lower particle size limit, we performed STEM, shown in Figure 4. The ZnO nanoparticles were indicated by the arrows on the figure, pointing to the formation of nanoparticles at ∼1 nm particles size. Highly dispersed ZnO nanoparticles have also been previously observed on MgO-supported catalysts.[44,54] Isolated (monomeric) Cu sites, as well as oligomeric sites in both CuMg and CuMgSi, cannot be detected using STEM/EDS in Figure 4, indicating high dispersion of these sites.

To confirm the presence of some reduced species on the surface, oxidative treatment was done after helium pretreatment by flowing air (Figure S5). The significant increase in the CT bands at 250 and 310 nm at the expense of peaks at 575 and 633 nm for CuMgSi indicates the presence of some native reduced species that became oxidized upon the introduction of air at higher temperature. Similarly, ZnMgSi shows the continuous increase in peaks at 230 and 340 nm, indicating the formation of both MgSi sites and bulk ZnO phases when oxidized.

3.2. Steady State Catalytic Performance and Acid/Base Chemistry of the Catalyst Active Sites. The steady state reactivity comparison between MgSi, ZnMgSi, and CuMgSi catalysts is shown in Figure 5. Here the activity of three catalysts is compared in the temperature range of 350−

Table 1. Vibrational Frequencies in the 1600−1400 cm^{-1} Wavenumber Range and Their Assignments for Ethanol, Enolate, Acetaldehyde, Crotonaldehyde, and Crotyl Alcohol Adsorption on WK (1:1)[11]

	Experimental (cm^{-1})				
Assignment	Ethanol	Acetaldehyde	Enolate	Crotonaldehyde	Crotyl alcohol
ν (C=C)			1600, 1578	1600, 1574	1602
δ (CH_2)	1454				1380
δ (CH_3)	1418			1456, 1434	1368
ρ_w (CH)	1380				
ρ_w (CH_2)					1441
ρ_w (CH_3)	1338	1456, 1434, 1382		1346	1456

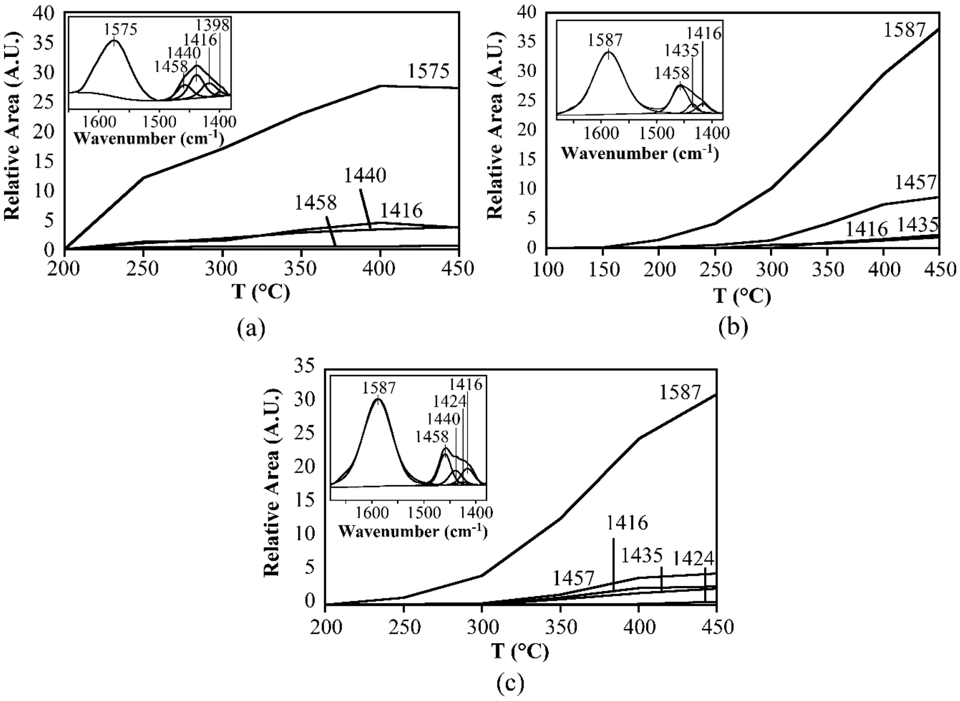

Figure 6. Evolution of each peak during *in situ* temperature-programmed ethanol DRIFTS over (a) MgSi, (b) CuMgSi, and (c) ZnMgSi. Insets: original spectra of ethanol DRIFTS from where the peaks were deconvoluted.

450 °C. It can be seen that promotion with Cu and Zn significantly enhanced the 1,3-BD formation rate from <1 mmol/g_{cat} h to ∼2 mmol/g_{cat} h throughout the investigated temperature range. Furthermore, ethylene formation was suppressed, more significantly in the case of Zn promotion. The origin of this promotional effect can be traced back to the production of acetaldehyde, which significantly increased in comparison to the unpromoted catalyst. The accumulation of acetaldehyde on the surface indicates that the rate-determining step (RDS) shifted for the case of promoted MgO/SiO_2. Quantitatively, this is confirmed by the decrease in apparent activation energy, E_a, as derived from the Arrhenius plot of each product formation rate. Acetaldehyde and 1,3-BD activation energies exhibit similar trends with promotion by Cu and Zn, with E_a (Zn) < E_a (Cu) < E_a (unpromoted). The apparent activation energy of ethylene, on the other hand, decreases with Cu promotion but not with Zn. The very low formation rate of ethylene must be due to the very low rate constant for ethylene formation, since raising the reaction temperature does not have a significant effect on the formation rate. A similar increase in 1,3-BD production was previously reported by other investigators.[3] For instance, Angelici et al. noticed a sharp increase (∼20%) in both ethanol conversion and 1,3-BD yield upon promoting the wet-kneaded catalyst with 1% CuO. The productivity of their catalyst was very similar to that reported here: 0.48 mmol g_{cat}^{-1} h^{-1} at 425 °C and WHSV = 1.1 h^{-1}.[14] When the reaction was carried out at more than 375 °C, the conversion over ZnMgSi approached 100%. This increase in conversion was previously observed when Zn was shown to provide more Lewis acidity and also suppressed the Brønsted acidity.[15,55] Zn-promoted catalysts, such as MgO/SiO_2[15] and talc,[13] were reported to increase both the conversion and selectivity toward 1,3-BD. The latter showed the same productivity as our catalyst, ∼ 1.1 mmol g_{cat}^{-1} h^{-1} at an even lower reaction temperature (300 °C) and a much higher WHSV (8.4 h^{-1}).

A fundamental acid−base study on both transition metal-promoted catalysts was carried out by both *in situ* and *ex situ* methods (section S1.2). *In situ* studies using propionic acid showed that all three catalysts possessed a very limited amount of strong basic sites and that promotion with transition metals further decreased the amount of strong basic sites. The propionic acid cofeeding experiment showed that 1,3-BD productivity did not recover to its original formation rate, which suggests the presence of some strong basic sites that maintain strong interaction with the leftover propionic acid.[2]

With the wet-kneaded support, the strong basic sites are limited and more medium basic sites are present. Both *in situ* CO_2 poisoning and DRIFTS studies confirmed the increased availability of the medium and weak basic sites. Our study aligns well with a previous study using deuterated chloroform, with Cu−Mg solid solution being thought of as the reason for fewer strong basic sites.[28] The *in situ* poisoning further unraveled the site requirements for every step of the reaction, i.e. acetaldehyde formation on weak basic sites, dehydration on any sites, and aldol condensation and Meerwein−Ponndorf−Verley (MPV) reduction on strong basic sites. The reduced amount of strong basic sites is also the origin of RDS shift from acetaldehyde formation to MPV reduction. The RDS for this reaction on unpromoted MgSi catalyst was previously assigned to acetaldehyde formation, which requires weak basic sites. Promotion with transition metal catalysts improved this by providing redox sites and limiting the amount of strong basic sites, and therefore further increasing the weak basic/strong basic sites ratio to improve the overall reactivity. Increasing the kinetics of the first step was shown to be very beneficial, since although the strong basic sites are now decreased, the next steps, i.e. aldol condensation and MPV reduction, were not severely hampered.

The total amount of acid sites was also reduced by promotion with Zn and Cu, as shown by both *in situ* NH_3 poisoning and NH_3-DRIFTS experiments. Ethylene formation was reduced by poisoning of the acid sites, while the origin of acetaldehyde formation rate reduction is the competitive bonding between the available Cu^{2+} to NH_3, since Cu catalysts are routinely investigated as SCR catalysts.[56,57] This is further supported by the recovered acetaldehyde production. The acetaldehyde production was accompanied by successive reduction of Cu^{2+} to Cu^0, as shown by *in situ* XANES (*vide infra*) and was potentially the reason its productivity decreased over time.

3.3. Active Sites under Operating Conditions.

3.3.1. Temperature-Programmed Infrared Spectroscopy Measurements (TP-DRIFTS). The effect of metal promoters on the ETB reaction mechanism was probed using *in situ* temperature-programmed (TP) DRIFTS. This allowed the study of surface species participating during the reaction. Experiments utilizing different probe molecules, i.e. ethanol, acetaldehyde, crotonaldehyde, and crotyl alcohol, were performed. Detailed assignments of the IR peaks can be found elsewhere.[11] Table 1 summarizes the peak assignments from experiments done on the MgSi catalyst. The *in situ* DRIFT spectra in the 1700 to 1300 cm^{-1} region of MgSi, ZnMgSi, and CuMgSi catalysts are shown in Figure 6 (insets). There were two very prominent peaks in the spectra at high reaction temperatures (>250 °C), i.e. ∼1575 and 1440 cm^{-1}, previously assigned to the products of acetaldehyde aldol condensation and polymerization.[11] A noticeable difference between the unpromoted and promoted spectra was the exact position of the two peaks. On promoted catalysts, the C═C stretch shifted to 1587 cm^{-1} while the prominent peak for the C−H bending was at 1458 cm^{-1}. The 1587 cm^{-1} peak location is identical in the case for both CuMgSi and ZnMgSi, which indicates a similar anchoring site on the catalysts. As will be discussed later, some of the magnesium forms solid solution with both Cu and Zn, which is possibly the binding site of the reaction product, given the identical peak location.

The C−H bending peak was very complex since every reactive intermediate has a C−H group. Peaks were deconvoluted using CasaXPS software suite version 2.3.18PR1.1[58] into several different components. On the unpromoted catalysts, this broad envelope was deconvoluted into four peaks, i.e. 1458, 1440, 1416, and 1398 cm^{-1}. The peak at 1458 cm^{-1} was formed more rapidly in the case of promoted catalysts, while peaks at 1435 and 1416 cm^{-1} lagged, compared to the unpromoted catalyst. The growth of the peak at 1458 cm^{-1}, previously assigned to acetaldehyde (δ CH_3) and crotonaldehyde (ρ_w CH_3), is significantly enhanced over promoted catalysts. The peaks at 1587−1575 and 1457 cm^{-1} can be used to characterize the degree of both aldol condensation and dehydrogenation that takes place on the surface, while the other peaks at ∼1400 cm^{-1} are characteristic of the catalyst' basicity, i.e. its ability to readily polymerize the formed acetaldehyde. This insight can be further utilized to probe the abundance of the active sites on the catalyst, i.e. based on the accumulated 2,4-hexadienal, which was characterized by the 1587 cm^{-1} peak. We carried out semiquantitative analysis of the peaks at 1587 (1575), 1440, and 1458 cm^{-1}. The peaks at ∼1400 cm^{-1} are summed together assuming that they result from a similar class of reaction, i.e. polymerization that typically yields more than one product such as metaldehyde and paraldehyde.[59] The evolution of these peaks as a function of temperature was plotted in Figure 6. It can be seen that for all catalysts, there was no significant changes in the ∼1400 cm^{-1} peak area. However, the promoted catalysts resulted in a higher intensity/area of the 1587 cm^{-1} peak with Cu higher than Zn. This indicates that promoting the catalyst with transition metals enhances the ability of the catalyst to carry out aldol condensation, while at the same time keeping the unwanted polymerization constant with regard to the unpromoted catalyst. Another noticeable difference was the temperature where the peak started increasing in intensity. For Cu, the peak starts increasing at lower temperature, even at ∼150 °C, while Zn lagged behind and eventually showed similar reactivity to the unpromoted catalyst.

Overall, combination of both DRIFTS and steady state fixed-bed experiments showed a shift in the rate-limiting step. Without the promotion with transition metals, less acetaldehyde was produced in the product stream, indicating the rapid consumption of the intermediate. Promoted catalysts, on the other hand, saw an increase in acetaldehyde production. The accumulation of acetaldehyde in the steady-state reaction experiments suggested that aldol condensation is the RDS. The acidity and basicity of the catalyst was affected by promotion with transition metals as well. The *in situ* poisoning experiment with propionic acid and NH_3 showed that promotion increased the availability of the weak basic sites and total acid sites. *In situ* DRIFTS detection of ethanol indicated that there was a change in the binding site during the aldol condensation, as manifested by the shift of the C═C stretch peak at 1575 to 1587 cm^{-1}. This systematic change suggested that while the anchoring site was identical between the two promoted catalysts, a potential solid solution formation took place. Mechanistically, this semiquantification confirms the steady-state experimental findings where the activation energy of the dehydrogenation step was significantly reduced leading to higher amounts of acetaldehyde and products of aldol condensation. The change in the polymerization products was also an indication of the reduced basicity of the catalyst, since acetaldehyde polymerization prevails on very basic surfaces.[60,61]

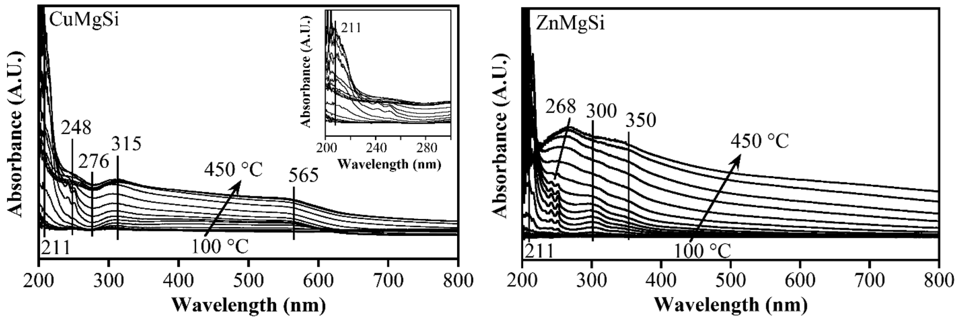

(a) (b)

Figure 7. *In situ* UV−vis DRS under constant ethanol flow over (a) CuMgSi and (b) ZnMgSi.

3.3.2. In Situ UV−vis DRS during Ethanol Reaction over MgSi Catalysts. Figure 7 shows the *in situ* UV−vis DR spectra during ethanol conversion to 1,3-BD on (a) CuMgSi and (b) ZnMgSi. The spectra plotted are difference spectra referenced to 100 °C to better describe the dynamic changes. Analysis with *in situ* UV−vis DRS further improved understanding of the interaction between catalyst and the surface intermediates. On CuMgSi, UV−vis DR spectra at lower temperature, i.e. 100−200 °C, did not exhibit any specific absorption bands. The first bands observed during the reaction were bands at 211, 248, and 315 nm. Increasing the temperature lead to intensity increases at 248, 315, and 565 nm while the band at 276 nm showed a decrease in intensity. Interestingly, the inset in Figure 7a shows that the band at 211 nm reached a maximum at 300 °C and decreased in intensity at higher temperature. To assist with the peak assignments, we performed similar experiments on an unpromoted MgO/SiO_2 catalyst (Figure S10). The UV−vis spectra of the unpromoted catalyst showed changes for three bands at 210, 245, and 300 nm. These three peaks can be assigned to either CT bands of metal oxides, $\pi-\pi^*$ transitions of allylic cations, cyclic or aromatic species, or even neutral, uncharged aromatic species (for shorter wavelengths).[62,63] The peak at 210 nm now corresponds to the peak at 211 nm in the case of CuMgSi and indicates the changes on the catalyst surface sites brought upon during the reaction. The behavior of this peak that changes with temperature, along with the shape of it, further indicated that this peak does not correspond to the abnormality of the system, i.e. low wavelength equipment limitation.

The peak at 248 nm was previously assigned to dienes that were observed in methanol-to-olefin (MTO) reaction on H-SAPO-34.[64] While reaction was not identical, some initial reaction steps are relevant. For instance, the dienes were observed when the reaction temperature was considerably low with only DME observed in the product stream. This could indicate that similar C−H bond activation step took place since ethanol dehydration to ethylene is also a competing reaction.[6,65] The peak at 315 nm, which increases linearly with increasing temperature, indicates the presence of monoenylic aromatic carbenium ions.[62,64] This finding is consistent with DRIFTS data where a peak due to the aromatic species continuously increased due to the production of higher aromatics and aldehydes. The remaining peak at 276 nm decreased at the expense of the peak at 565 nm. The former was assigned to oligomeric CuO species, while the latter one was assigned to surface plasmon resonance.[28,40] The presence of surface Cu^0 from reduced CuO oligomeric species will later be confirmed by X-ray methods since the peak at 565 nm could also originate from substituted or unsubstituted benzene (by)products.[62]

In situ experiment on ZnMgSi catalyst revealed a very different trend (Figure 7b). The bands are much broader in general than on CuMgSi. A similar peak at low wavelength at 211 nm indicates the change in the catalyst, and this suggested that the catalyst Mg−O−Si site was changing during the reaction since it happened on all catalysts tested. At low temperature there were two distinct peaks around 250 nm which slowly merged into one peak centered at 268 nm. These two peaks are assigned to dienes.[64] The peak at 248 nm was initially two peaks that merged into one. Hence, the peak at 268 nm is simply a convolution of two different dienes at 250 nm and a more intense species at around 268 nm. The peak at 268 nm intensified at higher temperature and was previously assigned to aromatics and polyalkylaromatics.[64] Similar to dienes that appeared at lower temperature, these surface species were also observed on MTO catalysts.[64,66] Mechanistically, formation of these species took very different pathways from the MTO since the MTO reaction pathway fully relies on the carbon pool from C−O bond scission and C−C bond formation. On the other hand ETB begins with dehydration and dehydrogenation of the alcohol and aldol condensation to form higher aromatics and aldehydes.

The formation of monoenylic carbenium ions, shown by the band at 300 nm, also occurred on ZnMgSi, although their formation was overshadowed by the band at 268 nm.[62,64,67−70] The peak is shifted from CuMgSi but at the same wavelength with unpromoted MgSi catalyst. This also indicates the similarity between ZnMgSi and MgSi in terms of binding site of the surface species. The band at 345 nm had a cutoff at 350 nm. While this was previously assigned to $\pi-\pi^*$ transitions of dienic allylic cations,[62,64,67−70] it is more likely that this band is due to bulk ZnO formation since its emergence was also accompanied by the intensity increase of a shoulder at ∼230 nm, which alternatively can be assigned to CT between Mg^{2+} to SiO_2.[27] The band at 400 nm is in particular very important in the case of MTO.[64,66,71−74] While the bands in this wavelength region are not as intense, the formation of polycyclic aromatics (400−410 nm) and trienylic carbenium ions (430−470 nm) evidently took place on the catalyst at higher temperatures.[62,64,67−70]

Similarities in the assignment of the bands between MgSi, CuMgSi, and ZnMgSi indicate similar reaction mechanism. From the spectra it is evident that the reactivity increased in the order MgSi < CuMgSi < ZnMgSi. The more intense broad bands of ZnMgSi align well with the reactivity study where

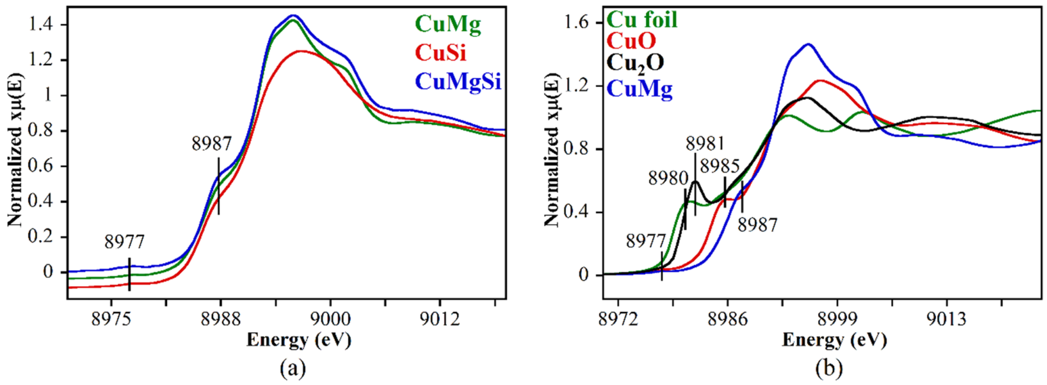

Figure 8. Normalized XANES spectra of CuMg, CuSi, and CuMgSi (a) and Cu foil, CuO, Cu_2O, and CuMg (b). XANES spectra in Figure 8(a) are offset vertically for clarity.

acetaldehyde dominates the vapor-phase. The produced acetaldehyde, when interacting with various reactive sites on the catalyst further leads to the formation of aromatic and polycyclic hydrocarbons bound on the catalyst, potentially deactivating it.

3.3.3. Operando XAS Studies of Cu, Zn-Promoted MgSi Catalysts. 3.3.3.1. Operando XANES and EXAFS of Cu-Promoted MgSi Catalyst. The XANES spectra of Cu catalysts and standards taken under ambient conditions are shown in Figure 8. The XANES spectra for samples with Cu-promoted supports, i.e. CuMg, CuSi, and CuMgSi, show similar features in the pre-edge region with a weak pre-edge peak located at about 8977 eV and a shoulder peak on the rising edge at about 8987 eV (Figure 8a). The weak feature at 8977 eV was previously assigned to the 1s → 3d transition and is considered a fingerprint of Cu^{2+} species.[28,75,76] For comparison, XANES spectra of the standards, i.e. Cu foil, Cu_2O, and CuO, are plotted along with the CuMg XANES spectrum in Figure 8b. The CuMgSi catalyst XANES spectrum strongly resembles that of the CuMg and is very different from CuSi (Figure 8a) and Cu standards (Figure 8b). Further, the EXAFS spectra (Figure S11) are very similar for both CuMg and CuMgSi. The shoulder peak at 8987 eV in the XANES spectrum of CuMg, when compared to CuO, was shifted from 8985 eV. This shoulder peak is usually assigned to the 1s → 4p transition, and its position is affected by the neighboring atomic geometry.[77] For CuMg, a shift in the shoulder peak was also observed.[28] Many reports attribute that shift to Cu being in octahedral or distorted octahedral geometry, occupying Mg lattice sites in a solid solution.[34,35,78]

As shown in Figure S12 (the Fourier transformed $k^2\chi(k)$ spectra of CuMg, Cu_2O, CuO, and Cu foil), the R-space EXAFS spectra of CuMgSi have two distinct peaks in the range of 1−3 Å. The peak at about 1.5 Å is due to the Cu−O contribution, and the peak at about 2.6 Å could be due to the Cu−Cu contribution from Cu oxides or the Cu−Mg contribution if Cu enters the MgO lattice. To determine the local environment of Cu, EXAFS data fitting analysis was performed. To fit the theoretical EXAFS signal to the experimental spectrum, two plausible models of local atomic arrangement around Cu absorbers were tested. Model A includes Cu−O and Cu−Cu nearest neighbor single-scattering paths, and Model B includes Cu−O and Cu−Mg paths. The fitting k range was 2.0−11.0 $Å^{-1}$, and the R range was 1.0−3.1 Å. The best fitting results were obtained when Model B was used. Only this model provided both reasonable results for the fitting parameters and good quality of the fit as shown in Figure S14. The best fitting results are shown in Table 2. For comparison, the structural parameters for Cu foil, CuO, Cu_2O, and MgO are also listed in Table 2. The Cu−O bond parameters for both samples are similar to those of the Cu−O bond in CuO. The Cu−Mg bond lengths in both CuMg and CuMgSi are also similar to the Mg−Mg and Cu−Cu bond lengths of MgO and CuO standards, respectively. The Cu−Cu contribution was not detected for either CuMg or CuMgSi, which corroborates the insertion of Cu into the MgO lattice. The coordination number of Cu−O shown in the EXAFS analysis was also in line with the (distorted) octahedral geometry. Previous investigations by Asakura et al. and Angelici et al. demonstrated that Cu−O coordination numbers were lower than 6.[28,34] Angelici et al. found a coordination number of 4 and further assumed the presence of two additional oxygen atoms to simulate the XANES spectra, which revealed another contribution from a Cu−O bond at ~2.40 Å, which is characteristic of the separation between copper and apical oxygen atom in a CuO_6 complex.[28] For CuMg, the Cu−O contribution follows similar observation of Angelici et al. and Asakura et al., i.e. less than 6.[28,34]

Table 2. Best Fitting Results of Cu Catalysts[a]

Sample	Bond	N	R (Å)
CuMgSi	Cu−O	5.6 ± 1.1	1.96 ± 0.02
	Cu−Mg	7.0 ± 1.8	3.01 ± 0.02
CuMg	Cu−O	4.5 ± 0.9	1.97 ± 0.02
	Cu−Mg	7.1 ± 2.0	3.00 ± 0.03
CuO	Cu−O	4	1.96
	Cu−O	2	2.78
	Cu−Cu	4	2.9
	Cu−Cu	4	3.08
	Cu−Cu	2	3.18
Cu_2O	Cu−O	2	1.84
	Cu−Cu	12	3.01
MgO	Mg−O	6	2.11
	Mg−Mg	12	2.98
Cu foil	Cu−Cu	12	2.56
	Cu−Cu	12	2.56

[a] The structural parameters of standards are listed for comparison.

Operando XAS experiments with flowing ethanol over CuMgSi were performed at different reaction temperatures to analyze the role of Cu species during the reaction, and at

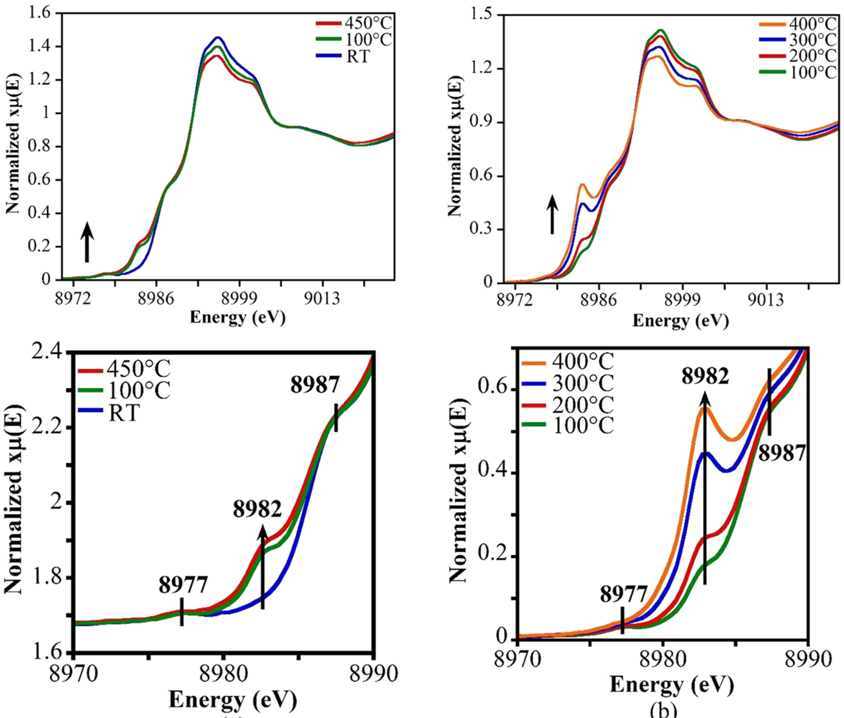

(a)

(b)

Figure 9. Normalized temperature-programmed *operando* XANES spectra of CuMgSi catalyst under He flow (a) and ethanol flow (b).

400 °C multiple scans were performed to investigate the evolution of Cu species as the reaction progresses at constant temperature. Figure 9 shows the XAS spectra of CuMgSi under both helium flow (a) and constant ethanol flow (b) at different temperatures. As shown in Figure 9, the pre-edge peak (at 8977 eV), which is a signature of Cu divalent species, remains almost unchanged after pretreatment, indicating Cu remains in the 2+ state after He treatment. Under helium at elevated temperatures, a new feature at 8982 eV appeared suggesting the change of the local environment of Cu after pretreatment. The position (8982 eV) of this peak is quite close to that (8981 eV) of the shoulder peak of Cu_2O, in which each Cu atom is surrounded by two O atoms in a collinear manner. The appearance of the 8982 eV peak thus implies a decrease in the average coordination number of the Cu−O bond for Cu atoms in the CuMgSi catalyst. During the experiment with ethanol, significant increase in the intensity of the 8982 eV peak was observed, especially at high temperatures, suggesting an increased fraction of species in which the average Cu−O coordination number is low. We propose that such geometry is correlated with catalytic activity of the CuMgSi catalyst. The corresponding mass spectrometry (MS) data (Figure S15) show that the acetaldehyde (AA) was produced at very low temperature, i.e. starting as low as 100 °C, and increased significantly at ~250 °C. This increase correlated with the significant increase in the 8982 eV peak observed in going from 200 to 300 °C in Figure 9. At the same time, the 1,3-BD started being produced at ~250 °C, which was lower than for the unpromoted catalyst, i.e. 300 °C.

When reaction temperature reached 400 °C, the temperature was held constant while XANES spectra were repeatedly taken to investigate any changes that take place during the reaction. The change in the copper species was recorded as a function of time for a total of ~2 h (Figure 10). A Cu foil XANES spectrum taken at ambient temperature was overlaid for comparison. As the reaction proceeded, the peak at 8982 eV started decreasing in intensity, suggesting the rearrangement of the local structure of Cu. Accompanied with this decrease, the peak at 8980 eV which is also a feature of the Cu foil spectrum appeared and increased with time, suggesting the formation of a Cu metallic phase. Based on the above results, we conclude that changes in the local structure of Cu occurred throughout the reaction. Quantitative information on the local structure of Cu during the reaction conditions was obtained by performing EXAFS analysis, and the results were summarized in Figure 11. It shows the change in the coordination numbers of Cu−Cu, Cu−Mg, and Cu−O bonds during the reaction. From 200 to 400 °C, a steady decrease in Cu−O bond coordination number takes place, which, as discussed above, also correlates with increase in the intensity of the 8982 eV peak. There was no appearance of a Cu−Cu pair until the steady-state reaction at 400 °C. At 400 °C, the final EXAFS spectra show a significant increase in Cu−Cu coordination number from 0 to about 3. This indicates clustering of the Cu atoms after reaction has stabilized at 400 °C.

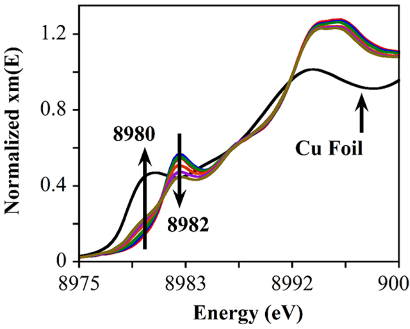

Figure 10. Normalized time-resolved *operando* XANES spectra of CuMgSi catalyst under ethanol flow at 400 °C.

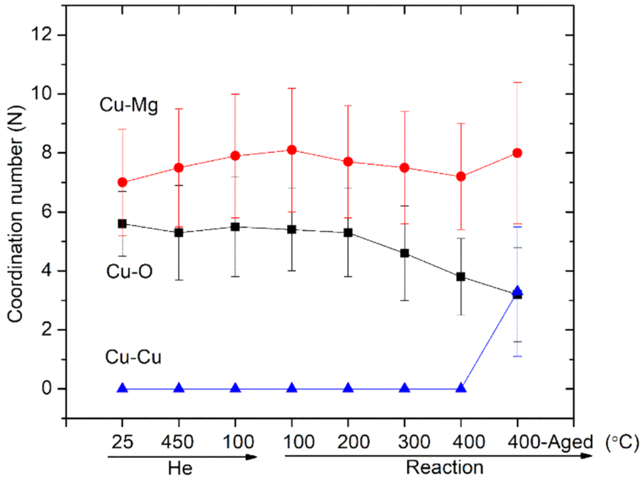

Figure 11. Coordination number changes during reaction of ethanol to 1,3-BD over CuMgSi.

To confirm the correlation between the XANES features and the coordination number of the Cu−O bond, XANES spectra simulations were performed using FEFF 9 code.[79] Simulations were first performed on CuO and Cu_2O to find optimized simulation parameters, which were then applied in calculating the spectra for all models. For the as-prepared CuMgSi catalyst, according to EXAFS analysis, the coordination number of Cu−O was close to 6 and Cu is very likely residing in the Mg sites in the MgO lattice. We simulated a MgO sphere with a diameter of about 1.6 nm and which contains 251 atoms and replaced the core Mg atom by a Cu atom. This model was named Model 1. In this model, Cu is octahedrally coordinated by 6 O atoms at the same distance. The calculated XANES spectrum for this model is plotted in Figure 12, and the shoulder peak at the rising edge is indeed shifted to higher energy compared to that of CuO, which agrees with the trend observed in the experimental data. As shown by the EXAFS results, under reaction conditions and at high temperatures, the average Cu−O coordination number decreases and is close to 4. We thus modified Model 1 by removing 2 oxygen atoms around Cu. In this modified model, Model 2, Cu is then surrounded by 4 oxygen atoms at the same distance forming a planar geometry. In the simulated XANES spectrum for Model 2, a shoulder peak appears in the position between those of Cu_2O and CuO. Such a trend was also observed in the experimental spectra. Therefore, the agreement between the experimental and theoretical XANES spectra suggests the shoulder peak at the rising edge of the Cu spectra is related to the local oxygen environment around Cu. In the CuMgSi system, Cu replaces Mg in the MgO lattice. When the reaction occurs, the octahedral Cu−O geometry will be distorted: most likely, part of oxygen atoms are pulling away from Cu, which could be then transformed to a Cu metallic phase as suggested by features detected for the final aged catalyst (Figure 10).

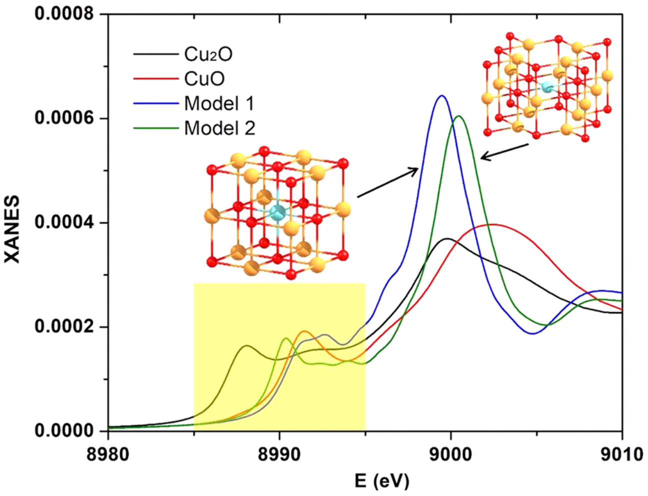

Figure 12. XANES spectra of the simulated CuO Model 1: Cu in a local environment surrounded by 6 oxygen atoms and Model 2: Cu in a local environment surrounded by 4 oxygen atoms. The features in the pre-edge region (highlighted) are discussed in detail in the text.

An alternative, complementary interpretation of this *operando* measurement was offered by Angelici et al., where reactions were carried out at 400 °C under two different pretreatment conditions, i.e. inert flow and reducing atmosphere.[28] Under inert flow, the initial state of the catalyst consisted of the native distorted octahedral Cu^{2+} species that was originally in the catalyst and another Cu^{2+} species that resembled to Cu^{2+} from CuO/SiO_2. This latter Cu^{2+} species was reduced to Cu^0 and transformed to a distorted octahedral Cu^{2+} species when pretreated at 425 °C under inert flow. Our observations show that there are new Cu species as evidenced by the peak at 8982 eV that appeared when the catalyst was pretreated at high temperature even though the pre-edge feature at 8977 eV, assigned to the distorted octahedral Cu^{2+} from CuMgSi, barely changed. Interestingly, a similar distribution between Cu^{2+}, Cu^+, and Cu^0 was observed after ethanol reaction without reducing pretreatment, after reducing pretreatment under H_2 and after ethanol reaction with reducing pretreatment.[28] Specifically, the three treatment steps mentioned correspond to increasing amount of Cu^0 in the final state of the catalyst. This indicates that both ethanol and hydrogen have a competing reducing effect on the catalyst. The final state after the steady-state reaction under both pretreatment conditions revealed that there were some Cu^{2+} species on the catalyst even after extensive reaction with ethanol.[28]

In our experiments, however, we observed a different outcome. The two pre-edge features at 8977 and 8987 eV behaved similarly with both of them barely changing during the reaction. Even after extensive reaction at 400 °C, the Cu−Mg coordination number did not change, while the Cu−O coordination number decreased (Figure 11) to 4. The apparent increase in peak at 8987 eV is mostly due to the increase in background from the peak at 8982 eV. We propose, based on data in Figures 9−12, that the origin of the peak at 8982 eV, assigned to Cu^{2+} with less-than-6 oxygen neighbors, is from a bulk Cu^{2+} with six oxygen neighbors that catalyzed the reduction and lost bonding with two neighbor oxygens during interaction with ethanol, as indicated by the simulation (Figure 12). Furthermore, this new Cu species undergoes a further change in coordination number, decreasing to reduced Cu^0, possibly due to the depletion of reducible Cu^{2+} that shifts the reaction active sites, which further leads to reduction of all reducible copper species into Cu^0, as suggested by clustering of Cu (increase in Cu−Cu coordination number) as the reaction progressed at 400 °C.

3.3.3.2. Operando XANES and EXAFS of Zn-Promoted MgSi Catalyst.

The XANES spectra of Zn catalysts and standards taken in ambient condition are shown in Figure 13a.

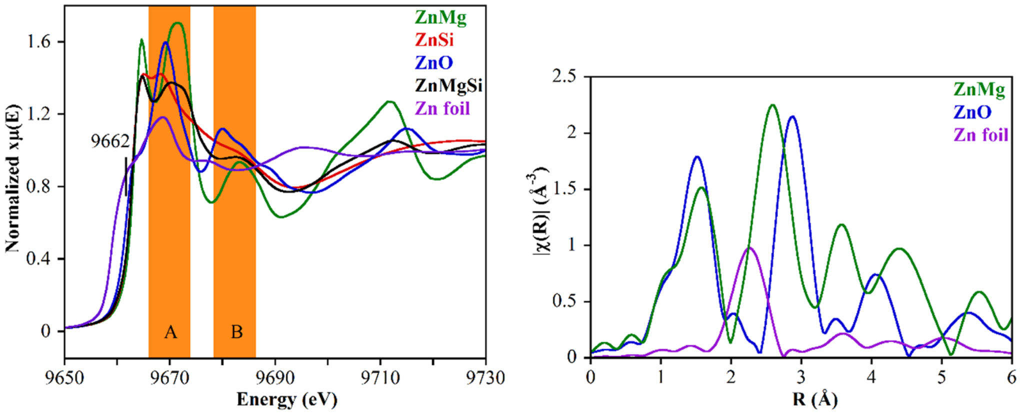

(a) (b)

Figure 13. (a) Normalized XANES spectra of ZnMg, ZnSi, ZnMgSi, Zn foil, and ZnO. (b) Fourier transforms of the EXAFS spectra of ZnMg, ZnO, and Zn foil.

The standards used in this study are Zn foil and ZnO to represent the reduced and oxidized states of the transition metal. Comparison between ZnMgSi, ZnSi (ZnO/SiO$_2$), and ZnMg (ZnO/MgO) reveals similarity between ZnMgSi and ZnMg. The silica-supported sample looks like those of willemite or hemimorphite, both Zn-silicates.[43] Chouillet et al. investigated the effect of drying temperature prior to calcination, and XANES spectra of all dried samples calcined at 450 °C, only 50 °C lower than our temperature, are nearly identical and indicative of zinc silicate formation.[43] The Zn foil exhibits a peak at 9662 eV, which was assigned to an electron transition to an empty d orbital. The absence of this feature indicates that all samples are fully oxidized.[80] For Zn standards (ZnO and Zn foil), there are two main features, the main edge, labeled as A, and feature B in the spectra. The main peak was assigned to a 1s → 4p electron transition with lesser peak intensity corresponding to decreasing coordination number of the cation.[81−83] The second feature was attributed to a multiple scattering resonance associated with medium range molecular structure around the target element; this feature was located differently for each sample, indicating a difference in geometric molecular structure.[81,82]

Both Mg-containing samples, i.e. ZnMg and ZnMgSi, exhibit splitting at the edge that was significantly larger than that of ZnSi. The splitting was previously observed on ZnO/Al$_2$O$_3$ and ZnFe$_2$O$_4$ and was attributed to a Zn^{2+} structure in a rigid environment nothing like ZnO.[82,84] EXAFS spectra of the samples show very similar spectral shape between the two samples although the oscillation magnitude of the ZnMgSi sample was much lower (Figure S13) . The similarity indicates that the Zn in both samples possess very similar local structure. Fourier transform was applied to the EXAFS signal ($k^2\chi(k)$) of ZnMg to represent both samples and compared to ZnO and Zn foil (Figure 13b). Between 1 and 3 Å, there are two peaks at 1.40 and 2.40 Å for ZnMg. From the Fourier transformed spectra the first peak was attributed to a Zn−O bond, while the latter was lower than the Zn−Zn distance in ZnO yet higher than the Zn−Zn distance in Zn foil. This implies that this was not due to a contribution from a Zn−Zn pair and instead we predict this to be due to a Zn−Mg pair. To confirm it, we did EXAFS analysis for the ZnMgSi catalyst and tested three models, analogously to what was described above for Cu edge analysis: Model A includes Zn−O and Zn−Zn paths; Model B includes Zn−O, Zn−Zn, and Zn−Mg paths; Model C includes Zn−O and Zn−Mg paths. The fitting k range is 2.0−10.5 Å^{-1}, and the R range is 1.0−3.2 Å. Only Model C yields both reasonable fitting results and good fit quality (Figure S14), which indicates that Zn was singly distributed into the MgO lattice. The best fitting results were summarized in Table 3.

Table 3. Best Fitting Results for ZnMgSi, ZnMg, ZnO, MgO, and Zn[a]

Sample	Bond	N	R (Å)
ZnMgSi	Zn−O	3.6 ± 0.5	1.98 ± 0.02
	Zn−Mg	4.8 ± 1.6	3.09 ± 0.04
ZnMg	Zn−O	4.7 ± 1.0	2.09 ± 0.04
	Zn−Mg	14.0 ± 2.8	3.05 ± 0.02
ZnO	Zn−O	4	1.94
	Zn−Zn	6	3.15
	Zn−Zn	6	3.2
MgO	Mg−O	6	2.11
	Mg−Mg	12	2.98
Zn foil	Zn−Zn	6	2.66
	Zn−Zn	6	2.88

[a]The structural parameters of standards are listed for comparison.

Within the MgO lattice, the first nearest neighbor of Zn is O, and the second nearest neighbor is Mg. The average coordination number of Zn−O is close to 4 and 5 for Zn−Mg, which is much smaller than the coordination number of Zn−Mg in ZnMg catalyst (Table 3). Furthermore, that may explain the weaker spectral intensity in near edge region of Zn edge in ZnMgSi catalyst compared to ZnMg catalyst (Figure 13a). This Zn−Mg distance was ~0.2 Å shorter than that of Zn−Zn pair in the ZnO foil, as which was previously determined for Zn$_{(1-x)}$Mg$_x$O alloy.[85] The bond length values for standards and samples are tabulated in Table 3.

The *operando* XANES spectra during ethanol conversion are presented in Figure 14. Similar to the study of CuMgSi, the experiment was conducted with increasing temperature under He (Figure 14a) and ethanol flow (Figure 14b). The MS data for the experiment (Figure S15b) shows similarities with that for CuMgSi. In particular, acetaldehyde was produced very early as well, following the induction time between ethanol flowing into the reactor and the product stream entering the MS. The production of 1,3-BD follows a similar trend; that is, it started being produced at lower temperature before really

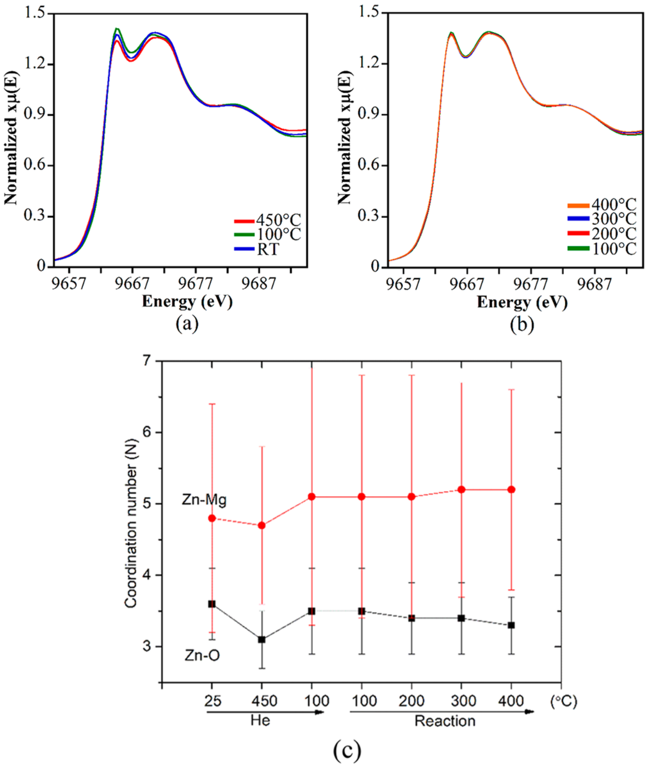

Figure 14. Normalized temperature-programmed *operando* XANES spectra of ZnMgSi catalyst under He flow (a) and ethanol flow (b). (c) Temperature-induced change in coordination number of Zn−Mg and Zn−O bonds during the reaction.

ramping up at ∼300 °C. This sudden increase at 300 °C coincides with a further increase in acetaldehyde production, which suggests that there are two active sites for ethanol dehydrogenation for each catalyst. The presence of these two sites on two promoted catalysts indicates that there are identical sites on both catalysts. When compared to the unpromoted MgSi catalyst, the steady-state activity testing data showed that acetaldehyde production was found to dramatically increase at this temperature as well. This indicates that promotion with Zn or Cu results in an additional dehydrogenating site and that the native weak basic sites responsible for the reaction are still present after promotion.

The Zn^{2+} local structure, however, has shown a resilient nature under flowing ethanol, as shown in Figure 14b. There was no significant change under ethanol flow, compared to the thermal effect when only helium flowed (Figure 14a). Figure 14c further showed the analysis of the EXAFS spectra where there were no significant changes in Zn local coordination number (N) during the reaction. The calculated Zn−Mg and Zn−O coordination numbers both remained constant and no change in the local state of the catalyst were observed. This indicates that the Zn-promoted catalyst should be relatively stable compared to the Cu-promoted catalyst and possible deactivation is more likely to be related to the formation of carbonaceous deposits on the surface due to the higher activity exhibited by the additional redox and Lewis acid sites provided by the Zn dopant.[15]

4. CONCLUSIONS

Cu- and Zn-promoted wet-kneaded MgO/SiO_2 catalysts were interrogated under *in situ* and *operando* conditions, providing new insights into the structure and reactivity of their catalytic sites during ethanol reaction to 1,3-BD. No distinct crystalline promoter phases were obtained according to XRD and STEM measurements, and Cu and Zn were suggested to bind strongly with the native OH groups. Under dehydrated conditions, oligomeric Cu−O species were found to dominate CuMgSi while the combination of very small <4 nm ZnO nanoparticles and possibly solid Zn solution with MgO has been observed using a combination of UV−vis and STEM measurements. A reduction in the amount of strong basic sites due to the metal promoter binding was found to affect RDS shift from acetaldehyde formation to MPV reduction. *In situ* DRIFT spectroscopy results allowed the decoupling of the aldol condensation and dehydrogenation fundamental steps that takes place on the surface, suggesting that transition metal promoters enhanced the ability of the catalyst to carry out aldol condensation, as supported by the steady state reactivity experimental results. *In situ* UV−vis spectroscopy suggested the appearance of $\pi-\pi^*$ electronic transitions of allylic cations, cyclic, or aromatic species on the catalysts while also providing insights on the oligomeric structure of the active sites. In particular, oligomeric CuO species with ∼0.8 Cu nearest neighbors were found to decrease in intensity suggesting their involvement in ultimate catalytic Cu^0 species formation.

Our *operando* X-ray measurements were combined with *ab initio* modeling to unravel the exact electronic structure of the Cu and Zn promoters. These measurements were performed as a function of temperature and signified that the Cu−Cu pair appeared at reaction temperatures of 400 °C on the aged (TOS of 6−7 h) catalyst at the expense of Cu−O bonds. Cu replaced Mg in the MgO lattice, which eventually led to Cu aggregation. This is akin to literature reports where deactivation of Cu-containing catalysts was suggested to be due to the carbonaceous deposits rather than sintering of the promoter. Furthermore, the 8982 eV peak typically assigned to Cu^+ species, in our work was assigned to a 4-fold coordinate Cu species rather than Cu_2O and is proposed to be the key intermediate leading to an increase in Cu−Cu pair number. This new Cu species is transient and is only populated at temperatures lower than 400 °C and starts decreasing to yield Cu^0 during aging with ethanol. Two types of Zn bonds, namely Zn−O and Zn−Mg, were identified during X-ray analysis and were resilient during conversion of ethanol under the operating conditions studied. Particularly, Zn was coordinated with about 4 oxygen neighbors at the distance of 1.98 Å and about 6 Mg neighbors at the distance of 3.09 Å.

Combination of the *in situ* and *operando* spectroscopic techniques in this study allowed us to identify the presence of several sites with different activities. In particular, the solid M−Mg (M = Cu, Zn) solution does not exhibit activities toward the reaction, while CuO and/or Cu−O−Cu (UV−vis) and ZnO (STEM) contributed to the dehydrogenation reactivity of both CuMgSi and ZnMgSi catalysts, respectively. The reducible nature of Cu led to its deactivation, as observed in the corresponding mass spectra data of the reactive intermediates, while Zn promoter demonstrated stability of the active site throughout the reaction.

■ ASSOCIATED CONTENT

Ⓢ Supporting Information

The Supporting Information is available free of charge on the ACS Publications website at DOI: 10.1021/acscatal.8b03515.

XRD patterns and *in situ* DRIFTS of selected references, Tauc plot of CuMgSi and its deconvolution, *in situ* UV−vis of oxidative dehydration of CuMgSi and ZnMgSi, *in situ* poisoning testing of reactivity and *in situ* DRIFTS using acid and base probe molecules aided by DFT of NH_3 adsorption on MgO slab, *in situ* UV−vis DRS of ethanol reaction on MgSi catalyst, EXAFS and R-space EXAFS spectra of catalysts and reference, EXAFS R-space simulation and fittings, and MS data of selected intermediates and products during the *operando* XANES-EXAFS of ETB on CuMgsi and ZnMgSi (PDF)

AUTHOR INFORMATION

Corresponding Author

*E-mail: job314@lehigh.edu. Phone: +1-610-758-6836.

ORCID

Anatoly I. Frenkel: 0000-0002-5451-1207

Jonas Baltrusaitis: 0000-0001-5634-955X

Present Address

○(W.E.T.) GEN-I, Surabaya, East Java 61213, Indonesia.

Author Contributions

∇W.E.T. and Y.L. contributed equally.

Notes

The authors declare no competing financial interest.

ACKNOWLEDGMENTS

W. T. and J. B. were supported by National Science Foundation under Grant No. CHE 1710120. A. I. F. and Y. L. were supported by the Division of Chemical Sciences, Geosciences, and Biosciences, Office of Basic Energy Sciences of the U.S. Department of Energy through Grant DE-FG02-03ER15476. Operations at the BL2-2 beamline at SSRL were made possible with the support of the Synchrotron Catalysis Consortium, funded by the U.S. Department of Energy Grant No. DE-SC0012335. *Operando* reactivity tests were supported by the LDRD 18-047 CO/EPS grant at Brookhaven National Laboratory. The authors gratefully acknowledge Israel E. Wachs for access to their UV−vis spectrometer and Arup Sengupta and Hang Dong for access to their ICP-OES. Lehigh University Professor John C. Chen Fellowship and P. C. Rossin Professorship are acknowledged. STEM images used Hitachi 2700C STEM of the Center for Functional Nanomaterials, which is a U.S. DOE Office of Science Facility, at Brookhaven National Laboratory under Contract No. DE-SC0012704.

REFERENCES

(1) Posada, J. A.; Patel, A. D.; Roes, A.; Blok, K.; Faaij, A. P. C.; Patel, M. K. Potential of Bioethanol as a Chemical Building Block for Biorefineries: Preliminary Sustainability Assessment of 12 Bioethanol-Based Products. *Bioresour. Technol.* **2013**, *135*, 490−499.

(2) Shylesh, S.; Gokhale, A. A.; Scown, C. D.; Kim, D.; Ho, C. R.; Bell, A. T. From Sugars to Wheels: The Conversion of Ethanol to 1,3-Butadiene over Metal-Promoted Magnesia-Silicate Catalysts. *ChemSusChem* **2016**, *9*, 1462−1472.

(3) Pomalaza, G.; Capron, M.; Ordomsky, V.; Dumeignil, F. Recent Breakthroughs in the Conversion of Ethanol to Butadiene. *Catalysts* **2016**, *6*, 203−237.

(4) Sushkevich, V. L.; Ivanova, I. I. Ag-Promoted ZrBEA Zeolites Obtained by Post-Synthetic Modification for Conversion of Ethanol to Butadiene. *ChemSusChem* **2016**, *9*, 2216−2225.

(5) Sushkevich, V. L.; Palagin, D.; Ivanova, I. I. With Open Arms: Open Sites of ZrBEA Zeolite Facilitate Selective Synthesis of Butadiene from Ethanol. *ACS Catal.* **2015**, *5*, 4833−4836.

(6) Taifan, W. E.; Bučko, T.; Baltrusaitis, J. Catalytic Conversion of Ethanol to 1,3-Butadiene on MgO: A Comprehensive Mechanism Elucidation Using DFT Calculations. *J. Catal.* **2017**, *346*, 78−91.

(7) Müller, P.; Burt, S. P.; Love, A. M.; McDermott, W. P.; Wolf, P.; Hermans, I. Mechanistic Study on the Lewis Acid Catalyzed Synthesis of 1,3-Butadiene over Ta-BEA Using Modulated Operando DRIFTS-MS. *ACS Catal.* **2016**, *6*, 6823−6832.

(8) Sushkevich, V. L.; Ivanova, I. I. Mechanistic Study of Ethanol Conversion into Butadiene over Silver Promoted Zirconia Catalysts. *Appl. Catal., B* **2017**, *215*, 36−49.

(9) Chieregato, A.; Velasquez Ochoa, J.; Bandinelli, C.; Fornasari, G.; Cavani, F.; Mella, M. On the Chemistry of Ethanol on Basic Oxides: Revising Mechanisms and Intermediates in the Lebedev and Guerbet Reactions. *ChemSusChem* **2015**, *8*, 377−388.

(10) Zhang, M.; Gao, M.; Chen, J.; Yu, Y. Study on Key Step of 1,3-Butadiene Formation from Ethanol on MgO/SiO2. *RSC Adv.* **2015**, *5*, 25959−25966.

(11) Taifan, W. E.; Yan, G. X.; Baltrusaitis, J. Surface Chemistry of MgO/SiO2 Catalysts during the Ethanol Catalytic Conversion to 1,3-Butadiene: In Situ DRIFTS and DFT Study. *Catal. Sci. Technol.* **2017**, *7*, 4648−4668.

(12) Fan, D.; Dong, X.; Yu, Y.; Zhang, M. A DFT Study on the Aldol Condensation Reaction on MgO in the Process of Ethanol to 1,3-Butadiene: Understanding the Structure-Activity Relationship. *Phys. Chem. Chem. Phys.* **2017**, *19*, 25671−25682.

(13) Hayashi, Y.; Akiyama, S.; Miyaji, A.; Sekiguchi, Y.; Sakamoto, Y.; Shiga, A.; Koyama, T.; Motokura, K.; Baba, T. Experimental and Computational Studies of the Roles of MgO and Zn in Talc for the Selective Formation of 1,3-Butadiene in the Conversion of Ethanol. *Phys. Chem. Chem. Phys.* **2016**, *18*, 25191−25209.

(14) Angelici, C.; Velthoen, M. E. Z.; Weckhuysen, B. M.; Bruijnincx, P. C. A. Effect of Preparation Method and CuO Promotion in the Conversion of Ethanol into 1,3-Butadiene over SiO2−MgO Catalysts. *ChemSusChem* **2014**, *7*, 2505−2515.

(15) Larina, O.; Kyriienko, P.; Soloviev, S. Ethanol Conversion to 1,3-Butadiene on ZnO/MgO−SiO2 Catalysts: Effect of ZnO Content and MgO:SiO2 Ratio. *Catal. Lett.* **2015**, *145*, 1162−1168.

(16) Da Ros, S.; Jones, M. D.; Mattia, D.; Pinto, J. C.; Schwaab, M.; Noronha, F. B.; Kondrat, S. A.; Clarke, T. C.; Taylor, S. H. Ethanol to 1,3-Butadiene Conversion by Using ZrZn-Containing MgO/SiO 2 Systems Prepared by Co-Precipitation and Effect of Catalyst Acidity Modification. *ChemCatChem* **2016**, *8*, 1−12.

(17) Ohnishi, R.; Akimoto, T.; Tanabe, K. Pronounced Catalytic Activity and Selectivity of MgO-SiO2-Na2O for Synthesis of Buta-1,3-Diene from Ethanol. *J. Chem. Soc., Chem. Commun.* **1985**, *No. 22*, 1613−1614.

(18) Sushkevich, V. L.; Ivanova, I. I.; Ordomsky, V. V.; Taarning, E. Design of a Metal-Promoted Oxide Catalyst for the Selective Synthesis of Butadiene from Ethanol. *ChemSusChem* **2014**, *7*, 2527−2536.

(19) Makshina, E. V.; Janssens, W.; Sels, B. F.; Jacobs, P. A. Catalytic Study of the Conversion of Ethanol into 1,3-Butadiene. *Catal. Today* **2012**, *198*, 338−344.

(20) Jones, M. D.; Keir, C. G.; Iulio, C.; Di; Robertson, R. A. M.; Williams, C. V.; Apperley, D. C. Investigations into the Conversion of Ethanol into 1,3-Butadiene. *Catal. Sci. Technol.* **2011**, *1*, 267−272.

(21) Bond, G. C.; Thompson, D. T. Catalysis by Gold. *Catal. Rev.: Sci. Eng.* **1999**, *41*, 319−388.

(22) Guan, Y.; Hensen, E. J. M. J. M. Ethanol Dehydrogenation by Gold Catalysts: The Effect of the Gold Particle Size and the Presence of Oxygen. *Appl. Catal., A* **2009**, *361*, 49−56.

(23) Wittcoff, H. A. A. Acetaldehyde: A Chemical Whose Fortunes Have Changed. *J. Chem. Educ.* **1983**, *60*, 1044.

(24) Sushkevich, V. L.; Ivanova, I. I.; Taarning, E. Mechanistic Study of Ethanol Dehydrogenation over Silica-Supported Silver. *ChemCatChem* **2013**, *5*, 2367−2373.

(25) Chang, F.-W.; Kuo, W.-Y.; Lee, K.-C. Dehydrogenation of Ethanol over Copper Catalysts on Rice Husk Ash Prepared by Incipient Wetness Impregnation. *Appl. Catal., A* **2003**, *246*, 253−264.
(26) Chang, F.-W.; Yang, H.-C.; Roselin, L. S.; Kuo, W.-Y. Ethanol Dehydrogenation over Copper Catalysts on Rice Husk Ash Prepared by Ion Exchange. *Appl. Catal., A* **2006**, *304*, 30−39.
(27) Janssens, W.; Makshina, E. V. V.; Vanelderen, P.; De Clippel, F.; Houthoofd, K.; Kerkhofs, S.; Martens, J. A. A.; Jacobs, P. A. A.; Sels, B. F. B. F. Ternary Ag/MgO-SiO2 Catalysts for the Conversion of Ethanol into Butadiene. *ChemSusChem* **2015**, *8*, 994−1008.
(28) Angelici, C.; Meirer, F.; van der Eerden, A. M. J.; Schaink, H. L.; Goryachev, A.; Hofmann, J. P.; Hensen, E. J. M.; Weckhuysen, B. M.; Bruijnincx, P. C. A. Ex Situ and Operando Studies on the Role of Copper in Cu-Promoted SiO2−MgO Catalysts for the Lebedev Ethanol-to-Butadiene Process. *ACS Catal.* **2015**, *5*, 6005−6015.
(29) Kyriienko, P. I.; Larina, O. V.; Soloviev, S. O.; Orlyk, S. M.; Calers, C.; Dzwigaj, S.; Pisarzhevsky, L. V. Ethanol Conversion into 1,3-Butadiene by Lebedev Method over MTaSiBEA Zeolites (M= Ag, Cu, Zn). *ACS Sustainable Chem. Eng.* **2017**, *5*, 2075−2083.
(30) Sekiguchi, Y.; Akiyama, S.; Urakawa, W.; Koyama, T.; Miyaji, A.; Motokura, K.; Baba, T. One-Step Catalytic Conversion of Ethanol into 1,3-Butadiene Using Zinc-Containing Talc. *Catal. Commun.* **2015**, *68*, 20−24.
(31) Baylon, R. a. L.; Sun, J.; Wang, Y. Conversion of Ethanol to 1,3-Butadiene over Na Doped ZnxZryOz Mixed Metal Oxides. *Catal. Today* **2016**, *259*, 446−452.
(32) Musolino, V.; Selloni, A.; Car, R. First Principles Study of Adsorbed Cun (N = 1−4) Microclusters on MgO(100): Structural and Electronic Properties. *J. Chem. Phys.* **1998**, *108*, 5044.
(33) Pacchioni, G. Supported Nickel and Copper Clusters on MgO(100): A First-Principles Calculation on the Metal/Oxide Interface. *J. Chem. Phys.* **1996**, *104*, 7329.
(34) Asakura, K.; Iwasawa, Y. A Structure Model as the Origin of Catalytic Properties of Metal-Doped MgO Systems. *Mater. Chem. Phys.* **1988**, *18*, 499−512.
(35) Colonna, S.; Arciprete, F.; Balzarotti, A.; Fanfoni, M.; De Crescenzi, M.; Mobilio, S. In Situ X-Ray Absorption Measurements of the Cu/MgO(001) Interface. *Surf. Sci.* **2002**, *512*, L341−L345.
(36) Rodriguez, J. a.; Jirsak, T.; Chaturvedi, S. Reaction of H2S with MgO(100) and Cu/MgO(100) Surfaces: Band-Gap Size and Chemical Reactivity. *J. Chem. Phys.* **1999**, *111*, 8077.
(37) Rodriguez, J. a.; Jirsak, T.; Freitag, A.; Larese, J. Z. Interaction of SO2 with MgO (100) and Cu/MgO (100): Decomposition Reactions and the Formation of SO3 and SO4. *J. Phys. Chem. B* **2000**, *2*, 7439−7448.
(38) Zhukovskii, Y. F.; Kotomin, E. a.; Borstel, G. Adsorption of Single Ag and Cu Atoms on Regular and Defective MgO(0 0 1) Substrates: An Ab Initio Study. *Vacuum* **2004**, *74*, 235−240.
(39) Matveev, A.; Neyman, K.; Yudanov, I.; Rösch, N. Adsorption of Transition Metal Atoms on Oxygen Vacancies and Regular Sites of the MgO(001) Surface. *Surf. Sci.* **1999**, *426*, 123−139.
(40) Bravo-Suarez, J. J.; Subramaniam, B.; Chaudhari, R. V. Ultraviolet-Visible Spectroscopy and Temperature-Programmed Techniques as Tools for Structural Characterization of Cu in CuMgAlOx Mixed Metal Oxides. *J. Phys. Chem. C* **2012**, *116*, 18207−18221.
(41) Ro, I.; Liu, Y.; Ball, M. R. R.; Jackson, D. H. K. H. K.; Chada, J. P. P.; Sener, C.; Kuech, T. F. F.; Madon, R. J. J.; Huber, G. W. W.; Dumesic, J. A. A. Role of the Cu-ZrO2 Interfacial Sites for Conversion of Ethanol to Ethyl Acetate and Synthesis of Methanol from CO2 and H2. *ACS Catal.* **2016**, *6*, 7040−7050.
(42) Vlaic, G.; Bart, J. C. J. C. J.; Cavigiolo, W.; Mobilo, S. X-Ray Absorption near Edge Structures (Xanes) of Cu/ZnO/Al2O3 Co Shift Catalysts. *Chem. Phys. Lett.* **1980**, *76*, 453−459.
(43) Chouillet, C.; Villain, F.; Kermarec, M.; Lauron-Pernot, H.; Louis, C. Relevance of the Drying Step in the Preparation by Impregnation of Zn/SiO2 Supported Catalysts. *J. Phys. Chem. B* **2003**, *107*, 3565−3575.
(44) Didenko, O. Z.; Kosmambetova, G. R.; Strizhak, P. E. Synthesis of Nanosized ZnO/MgO Solid and Its Catalytic Activity for CO Oxidation. *Chin. J. Catal.* **2008**, *29*, 1079−1083.
(45) Kvisle, S.; Aguero, A.; Sneeden, R. P. A. Transformation of Ethanol into 1,3-Butadiene over Magnesium Oxide/Silica Catalysts. *Appl. Catal.* **1988**, *43*, 117−131.
(46) Clausen, B. S. S.; Steffensen, G.; Fabius, B.; Villadsen, J.; Feidenhans'l, R.; Topsøe, H. In Situ Cell for Combined XRD and On-Line Catalysis Tests: Studies of Cu-Based Water Gas Shift and Methanol Catalysts. *J. Catal.* **1991**, *132*, 524−535.
(47) Chung, S.-H.; Angelici, C.; Hinterding, S. O. M.; Weingarth, M.; Baldus, M.; Houben, K.; Weckhuysen, B. M.; Bruijnincx, P. C. A. On the Role of Magnesium Silicates in Wet-Kneaded Silica-Magnesia Catalysts for the Lebedev Ethanol-to- Butadiene Process. *ACS Catal.* **2016**, *6*, 4034−4045.
(48) Chizallet, C.; Costentin, G.; Che, M.; Delbecq, F.; Sautet, P.; Surface, D.; Marie, P. Infrared Characterization of Hydroxyl Groups on MgO : A Periodic and Cluster Density Functional Theory Study Infrared Characterization of Hydroxyl Groups on MgO : A Periodic and Cluster Density Functional Theory Study. *J. Am. Chem. Soc.* **2007**, *129* (No. 19), 6442−6452.
(49) Gawande, M. B.; Goswami, A.; Felpin, F.-X.; Asefa, T.; Huang, X.; Silva, R.; Zou, X.; Zboril, R.; Varma, R. S. Cu and Cu-Based Nanoparticles: Synthesis and Applications in Catalysis. *Chem. Rev.* **2016**, *116*, 3722−3811.
(50) Marion, M. C.; Garbowski, E.; Primet, M. Physicochemical Properties of Copper Oxide Loaded Alumina in Methane Combustion. *J. Chem. Soc., Faraday Trans.* **1990**, *86*, 3027−3032.
(51) Coluccia, S.; Lavagnino, S.; Marchese, L. The Hydroxylated Surface of MgO Powders and the Formation of Surface Sites. *Mater. Chem. Phys.* **1988**, *18*, 445−464.
(52) Yoshida, H.; Shimizu, T.; Murata, C.; Hattori, T. Highly Dispersed Zinc Oxide Species on Silica as Active Sites for Photoepoxidation of Propene by Molecular Oxygen. *J. Catal.* **2003**, *220*, 226−232.
(53) Cavalleri, M.; Pelmenschikov, A.; Morosi, G.; Gamba, A.; Coluccia, S.; Martra, G. *Dissociative Adsorption of H2 on Defect Sites of MgO: A Combined IR Spectroscopic and Quantum Chemical Study*. In *Oxide-based Systems at the Crossroads of Chemistry Second International Workshop October 8−11, 2000, Como, Italy*; Gamba, A., Coluccia, S., Ed.; Elsevier, 2001; Vol. *140*, pp 131−139.
(54) Valizadeh, H.; Azimi, A. A. ZnO/MgO Containing ZnO Nanoparticles as a Highly Effective Heterogeneous Base Catalyst for the Synthesis of 4H-Pyrans and Coumarins in [Bmim]BF4. *J. Iran. Chem. Soc.* **2011**, *8*, 123−130.
(55) De Baerdemaeker, T.; Feyen, M.; Müller, U.; Yilmaz, B.; Xiao, F.-S.; Zhang, W.; Yokoi, T.; Bao, X.; Gies, H.; De Vos, D. E. Bimetallic Zn and Hf on Silica Catalysts for the Conversion of Ethanol to 1,3-Butadiene. *ACS Catal.* **2015**, *5*, 3393−3397.
(56) Liu, Q.; Liu, Z.; Li, C. Adsorption and Activation of NH3 during Selective Catalytic Reduction of NO by NH3. *Chin. J. Catal.* **2006**, *27*, 636−646.
(57) Díaz, G.; Pérez-Hernández, R.; Gómez-Cortés, A.; Benaissa, M.; Mariscal, R.; Fierro, J. L. G. CuO−SiO2 Sol−Gel Catalysts: Characterization and Catalytic Properties for NO Reduction. *J. Catal.* **1999**, *187*, 1−14.
(58) Baltrusaitis, J.; Mendoza-Sanchez, B.; Fernandez, V.; Veenstra, R.; Dukstiene, N.; Roberts, A.; Fairley, N. Generalized Molybdenum Oxide Surface Chemical State XPS Determination via Informed Amorphous Sample Model. *Appl. Surf. Sci.* **2015**, *326*, 151−161.
(59) Ordomsky, V. V.; Sushkevich, V. L.; Ivanova, I. I. Study of Acetaldehyde Condensation Chemistry over Magnesia and Zirconia Supported on Silica. *J. Mol. Catal. A: Chem.* **2010**, *333*, 85−93.
(60) Georgieff, K. K. Spontaneous Polymerization of Acetaldehyde to Polyacetaldehyde at Close to Dry-Ice Temperature. *J. Appl. Polym. Sci.* **1966**, *10*, 1305−1313.
(61) Bevington, J. C.; Norrish, R. G. W. The Polymerization of Acetaldehyde at Low Temperatures. *Proc. R. Soc. London, Ser. A* **1949**, *196*, 363 LP−378.

(62) Wulfers, M. J.; Tzolova-Müller, G.; Villegas, J. I.; Murzin, D. Y.; Jentoft, F. C. Evolution of Carbonaceous Deposits on H-Mordenite and Pt-Doped H-Mordenite during n-Butane Conversion. *J. Catal.* **2012**, *296*, 132−142.

(63) Nordvang, E. C.; Borodina, E.; Ruiz-Martínez, J.; Fehrmann, R.; Weckhuysen, B. M. Effects of Coke Deposits on the Catalytic Performance of Large Zeolite H-ZSM-5 Crystals during Alcohol-to-Hydrocarbon Reactions as Investigated by a Combination of Optical Spectroscopy and Microscopy. *Chem. - Eur. J.* **2015**, *21*, 17324−17335.

(64) Jiang, Y.; Huang, J.; Reddy Marthala, V. R.; Ooi, Y. S.; Weitkamp, J.; Hunger, M. In Situ MAS NMR-UV/Vis Investigation of H-SAPO-34 Catalysts Partially Coked in the Methanol-to-Olefin Conversion under Continuous-Flow Conditions and of Their Regeneration. *Microporous Mesoporous Mater.* **2007**, *105*, 132−139.

(65) Taifan, W. E.; Baltrusaitis, J. In-Situ Spectroscopic Insights on the Molecular Structure of the MgO/SiO 2 Catalytic Active Site During Ethanol Conversion to 1,3-Butadiene. *J. Phys. Chem. C* **2018**, *122*, 20894−20906.

(66) Wulfers, M. J.; Jentoft, F. C. The Role of Cyclopentadienium Ions in Methanol-to-Hydrocarbons Chemistry. *ACS Catal.* **2014**, *4*, 3521−3532.

(67) Kiricsi, I.; Förster, H.; Tasi, G.; Nagy, J. B. Generation, Characterization, and Transformations of Unsaturated Carbenium Ions in Zeolites. *Chem. Rev.* **1999**, *99*, 2085−2114.

(68) Ahmad, R.; Melsheimer, J.; Jentoft, F. C.; Schlögl, R. Isomerization of N-Butane and of n-Pentane in the Presence of Sulfated Zirconia: Formation of Surface Deposits Investigated by in Situ UV−vis Diffuse Reflectance Spectroscopy. *J. Catal.* **2003**, *218*, 365−374.

(69) Stepanenko, Y.; Sobolewski, A. L.; Mordziński, A. Electronic Spectroscopy and Methyl Internal Rotation Dynamics of 9,10-Dimethylanthracene. *J. Mol. Spectrosc.* **2005**, *233*, 15−22.

(70) Yang, S.; Kondo, J. N.; Domen, K. Formation of Alkenyl Carbenium Ions by Adsorption of Cyclic Precursors on Zeolites. *Catal. Today* **2002**, *73*, 113−125.

(71) Qian, Q.; Vogt, C.; Mokhtar, M.; Asiri, A. M.; Al-Thabaiti, S. A.; Basahel, S. N.; Ruiz-Martínez, J.; Weckhuysen, B. M. Combined Operando UV/Vis/IR Spectroscopy Reveals the Role of Methoxy and Aromatic Species during the Methanol-to-Olefins Reaction over H-SAPO-34. *ChemCatChem* **2014**, *6*, 3396−3408.

(72) Mores, D.; Kornatowski, J.; Olsbye, U.; Weckhuysen, B. M. Coke Formation during the Methanol-to-Olefin Conversion: In Situ Microspectroscopy on Individual H-ZSM-5 Crystals with Different Brønsted Acidity. *Chem. - Eur. J.* **2011**, *17*, 2874−2884.

(73) Mores, D.; Stavitski, E.; Kox, M. H. F.; Kornatowski, J.; Olsbye, U.; Weckhuysen, B. M. Space- And Time-Resolved in-Situ Spectroscopy on the Coke Formation in Molecular Sieves: Methanol-to-Olefin Conversion over H-ZSM-5 and H-SAPO-34. *Chem. - Eur. J.* **2008**, *14*, 11320−11327.

(74) VanSpeybroeck, V.; Hemelsoet, K.; DeWispelaere, K.; Qian, Q.; VanderMynsbrugge, J.; DeSterck, B.; Weckhuysen, B. M.; Waroquier, M. Mechanistic Studies on Chabazite-Type Methanol-to-Olefin Catalysts: Insights from Time-Resolved UV/Vis Microspectroscopy Combined with Theoretical Simulations. *ChemCatChem* **2013**, *5*, 173−184.

(75) Kang, M.; Park, E. D.; Kim, J. M.; Yie, J. E. Cu-Mn Mixed Oxides for Low Temperature NO Reduction with NH3. *Catal. Today* **2006**, *111*, 236−241.

(76) Xu, R.; Wei, W.; Li, W. H.; Hu, T. D.; Sun, Y. H. Fe Modified CuMnZrO2catalysts for Higher Alcohols Synthesis from Syngas: Effect of Calcination Temperature. *J. Mol. Catal. A: Chem.* **2005**, *234*, 75−83.

(77) Choy, J.-H.; Kim, D.-K.; Hwang, S.-H.; Demazeau, G. Cu K-Edge x-Ray-Absorption Spectroscopic Study on the Octahedrally Coordinated Trivalent Copper in the Perovskite-Related Compounds La2Li0.5Cu0.5O4 and LaCuO3. *Phys. Rev. B: Condens. Matter Mater. Phys.* **1994**, *50*, 16631−16639.

(78) Pascual, J. L.; Savoini, B.; González, R. Electronic Absorption Spectra of Cu2+ in MgO : Ab Initio Theory and Experiment. *Phys. Rev. B: Condens. Matter Mater. Phys.* **2004**, *70*, 045109.

(79) Rehr, J. J.; Kas, J. J.; Vila, F. D.; Prange, M. P.; Jorissen, K. Parameter-Free Calculations of X-Ray Spectra with FEFF9. *Phys. Chem. Chem. Phys.* **2010**, *12*, 5503−5513.

(80) Harvey, J. N. *DFT Computation of Relative Spin-State Energetics of Transition Metal Compounds BT - Principles and Applications of Density Functional Theory in Inorganic*; Chemistry, I., Kaltsoyannis, N., McGrady, J. E., Eds.; Springer Berlin Heidelberg: Berlin, Heidelberg, Heidelberg, 2004; pp 151−184.

(81) Galoisy, L.; Cormier, L.; Calas, G.; Briois, V. Environment of Ni, Co and Zn in Low Alkali Borate Glasses: Information from EXAFS and XANES Spectra. *J. Non-Cryst. Solids* **2001**, *293−295*, 105−111.

(82) Wang, H.-C.; Wei, Y.-L.; Yang, Y.-W.; Lee, J.-F. XAS Study of Zn-Doped Al2O3 after Thermal Treatment. *J. Electron Spectrosc. Relat. Phenom.* **2005**, *144−147*, 817−819.

(83) Kelly, R. A.; Andrews, J. C.; DeWitt, J. G. An X-Ray Absorption Spectroscopic Investigation of the Nature of the Zinc Complex Accumulated in Datura Innoxia Plant Tissue Culture. *Microchem. J.* **2002**, *71*, 231−245.

(84) Waychunas, G. A.; Fuller, C. C.; Davis, J. A.; Rehr, J. J. Surface Complexation and Precipitate Geometry for Aqueous Zn(II) Sorption on Ferrihydrite: II. XANES Analysis and Simulation. *Geochim. Cosmochim. Acta* **2003**, *67*, 1031−1043.

(85) Jeong, E.-S.; Park, C.; Jin, Z.; Yoo, J.; Yi, G.-C.; Han, S.-W. Orientation-Dependent Local Structural Properties of Zn1-x MgxO Nanorods Studied by Extended X-Ray Absorption Fine Structure. *J. Nanosci. Nanotechnol.* **2013**, *13*, 1880−1883.